Energy Storage Materials 16 (2019) 126–145

Contents lists available at ScienceDirect

Energy Storage Materials

journal homepage: www.elsevier.com/locate/ensm

Carbon electrodes for capacitive technologies

Paula Ratajczak[a,*], Matthew E. Suss[b], Friedrich Kaasik[c], François Béguin[a]

[a] Institute of Chemistry and Technical Electrochemistry, Poznan University of Technology, 60-965 Poznan, Poland
[b] Faculty of Mechanical Engineering, Technion – Israel Institute of Technology, Haifa 32000, Israel
[c] IMS Laboratory, Institute of Technology, University of Tartu, 50411 Tartu, Estonia

ARTICLE INFO

Keywords:
Carbon materials
Electrical double-layer capacitors
Energy storage and harvesting
Capacitive deionization and actuation
Potential controlled chromatography

ABSTRACT

An overview of capacitive technologies based on carbon materials (energy storage in electrical double-layer capacitors (EDLCs), capacitive deionization (CDI), energy harvesting, capacitive actuation, and potential controlled chromatography) is presented. The review reveals the role of carbon for these scientific and industrial purposes with disclosing the benefits and limitations of various nanostructured carbons for a certain application. A special attention is placed on the electrical double-layer (EDL) formation mechanisms affected by the porous texture of carbon and the electrode architecture. The importance of a careful selection of the electrolytic solution for the EDL formation inside the intraparticle pores of carbon electrodes is also enlightened.

1. Introduction

During the last fifty years, the worldwide industrial development accompanied by improving wealth in emerging markets and growth of the human population have driven a steadily increasing demand for new energy and fresh water supplies. The emission of noxious gases during fossil fuel consumption and the depletion of their reserves have led to introduce renewables (sun and wind) in the energy mix. Unfortunately, due to their intermittent character, the renewable technologies are not able to ensure a real-time balance of electricity supply [1]. Therefore, in order to adapt the energy delivery to the demand and improve the energy efficiency, current researches are focused on introducing energy-storage technologies which would meet sustainability, environmental requirements and be cost-effective. What is more, the automotive industry faces the challenge to reduce the exhaust gases emission and amount of energy dissipated in urban areas by internal combustion engine powered vehicles. Encouraging efficient energy management should accelerate commercialization of the power-train technologies to be applied in low carbon vehicles (LCV), fast-charging infrastructures in the stations, wireless monitoring systems or electricity load leveling in stationary and transportation systems. Apart from energy related issues, another critical problem worldwide concerns the shrinking access to potable water sources. It is commonly known that sea or brackish water is not suitable to drink without being desalinated. Therefore, alternative options to i.e. expensive vacuum distillation processes, reverse osmosis and cogeneration desalination plants, using either fossil fuels or nuclear power, are still highly sought in order to meet the global needs for clean water with reduced carbon footprint.

Electrochemical technologies are able to bring some response to the issues related with efficient energy management, reduction of green-house gases emissions and water desalination by utilizing the concept of electrical double-layer (EDL) created at the surface of nanoporous electrodes [2–4]. When an electrode is polarized, the ions of opposite charge present in the electrolyte migrate to the electrode surface, where they create an EDL [5]. The double-layer capacitance depends on the electrode surface area able to accumulate electrical charge by pure electrostatic forces and on the charge separation distance imposed by dimensions of the charge carriers. Therefore, electrodes made from nanostructured carbon materials (also called carbons further in the text), characterized by a highly extended surface area and pores which match with the size of electrolyte ions, are generally considered to be capacitive [4,6–13]. The capacitive technologies include: i) capacitive energy storage in electrical double-layer capacitors (EDLCs) [14,15]; ii) capacitive energy harvesting where small amount of ambient energy is captured, accumulated, and converted into electrical energy [16,17]; and iii) capacitive deionization (CDI) of sea or brackish water where the salt ions are removed from the feed water, electrostatically held in the EDL and released in a brine stream during discharge [18–20]. Besides, the charge-dependent ions separation can be also employed in a new type of liquid chromatography (called potential-controlled chromatography) to enhance the anolyte concentration or to introduce withholding of certain species [21]. What is more, the distribution of electric charges within the porosity of carbon material entails changes

* Corresponding author.
E-mail address: paula.ratajczak@put.poznan.pl (P. Ratajczak).

https://doi.org/10.1016/j.ensm.2018.04.031
Received 21 December 2017; Received in revised form 17 April 2018; Accepted 28 April 2018
Available online 01 May 2018

of geometric surface area of the electrodes triggered by charging and discharging, so-called capacitive actuation. The flexible capacitive devices where the electrodes deformation is controlled by a voltage stimulation can be used in soft robotics to make shape-changing robots [22].

In this context, the paper reveals the benefits and limitations of various nanostructured carbons, with a special attention to the charge storage mechanism in EDLCs affected by the porous texture of carbon electrodes. It then reviews the state-of-the-art of capacitive technologies based on carbon materials with discussing in some detail how the double-layer concept is being utilized for their development.

2. Theory and basics of the electrical double-layer

Considering the capacitive technologies, the formation of an electrical double-layer (EDL) at the electrode/electrolyte interface is the cornerstone to provide energy storage, harvesting, water desalination, actuation and potential controlled chromatography. Over the last two centuries, scientists have developed various models of the EDL describing the phenomena which occur at the solid conductor-electrolyte boundary and in its vicinity. On the example of a negatively polarized electrode, Helmholtz suggested that the interface consists of two electrical layers which are: (i) electrons at the surface of the electrode, (ii) and a monolayer of cations in the electrolytic solution [23]. According to this double-layer model, the specific capacitance C_{dl} is a constant value, according to formula (1):

$$C_{dl} = \frac{\varepsilon_r \varepsilon_0 S}{d} \tag{1}$$

where S is the surface area of the electrode/electrolyte interface, ε_r is the relative permittivity of the electrolyte, ε_0 is vacuum permittivity ($\varepsilon_0 = 8.854 \cdot 10^{-12}$ F m^{-1}), and d is the charge separation distance [14]. When considering flat surface electrodes where the average charge separation distance is around 1 nm, the specific capacitance C_{dl} is in the range of 30–70 μF cm^{-2} in the most commonly used solvents such as water (for which the dielectric constant ε_r is ~ 80.1), acetonitrile (AN, ε_r is ~ 37.5) and propylene carbonate (ε_r is ~ 64) [24]. However, C_{dl} at the porous carbon surface/electrolyte interface is in the range of 5–20 μF cm^{-2} due to various matching parameters (see Section 3) [25].

One of the shortcomings of the Helmholtz model is the assumption of ion accumulation into a single plane along the electrode surface. It does not take into account that, due to diffusion, ions do not accumulate at the surface of the electrode but form a diffuse space charge. Therefore, in the 1900s Gouy and Chapman formulated a model according to which the capacitance depends also on the applied potential and bulk ionic strength I [26], and is expressed by the Eq. (2):

$$C_{GC} = \frac{\varepsilon \kappa}{4\pi} \cosh \frac{z}{2} \tag{2}$$

where κ^{-1} is the Debye-Hückel length (nm) described in Eq. (3):

$$\kappa^{-1} = \sqrt{\frac{\varepsilon k T}{2 N_A e I}}, \tag{3}$$

I is the ionic strength of the electrolyte (mol m^3), N_A is the Avogadro number, e is the elementary charge, T is the absolute temperature (K), and k is the Boltzmann constant (1.3806488 10^{-23} J K^{-1}).

More than twenty years later, Stern included in his model both a compact and a diffuse layer [27], while Grahame divided this combined Stern layer into two regions: (i) a layer of adsorbed ions at the surface of the electrode, referred to as the inner Helmholtz plane (IHP) (ii) and an outer Helmholtz plane (OHP) formed by the diffuse ions in the vicinity of the electrode surface [28]. From the Grahame model, the capacitance C of the double-layer is described by Eq. (4):

$$\frac{1}{C_G} = \frac{1}{C_H} + \frac{1}{C_{GC}} \tag{4}$$

with C_H corresponding to the specific capacitance of the Helmholtz' compact double-layer, and C_{GC} resulting from the diffuse layer described by Gouy and Chapman.

For modern capacitive devices, this model is not applicable for several reasons, especially because it does not take into account the EDL structure in confined areas (e.g. micropores of porous carbons), or steric effects in the diffuse layer occurring at high surface potentials. Modern EDL models employ Donnan approximations for highly confined geometries occurring in capacitive electrodes [29], condensed layers and Bikerman lattice models to consider steric effects in the diffuse layer [30,31], or a Frumkin-Butler-Volmer model of Faradaic reaction kinetics coupled to EDL structure models for pseudocapacitive behavior [32]. Another currently used model of the electrical double-layer was described by Bockris, Devanathan and Müller (BDM model) [33], and proposes that a water layer with aligned dipoles is present at the surface of the electrode. Moreover, it is suggested that some water molecules are displaced by specifically adsorbed ions (e.g., redox ions) which can contribute to a pseudocapacitive effect. As presented on the example of a negatively polarized electrode (Fig. 1), the inner Helmholtz plane (IHP) passes through the centers of the specifically adsorbed ions and solvent molecules, which are oriented parallel to the electric field. Then, the outer Helmholtz plane (OHP) passes through the solvated ions centers, which are outside the IHP. Behind the outer Helmholtz plane, there is a diffuse layer region. The BMD model may be extended to the charge-transfer reactions occurring in organic electrolytes with polar solvents, for example, acetonitrile (AN), contributing to the potential drop across the electrode/electrolyte plane.

As already mentioned, the energy storage in capacitive technologies is based on the ability to store charge in the form of an EDL at the surface of polarized electrodes. Therefore, many researches are focused to increase the specific capacitance C_{dl} either by applying an electrolyte of high permittivity, or by choosing an electrode material characterized by an enhanced specific surface area S and low charge separation distance d (see Eq. (1)). Compared to flat metal plates, porous carbon electrodes are characterized by very high specific surface area (500–3000 m^2 g^{-1}) and extremely short charge separation distance (0.3–0.8 nm) at the electrode–electrolyte interface [34]. The slightly lower conductivity of some carbon materials can be easily compensated by using a good percolator and by an appropriate electrode manufacturing process. Nevertheless, it is important to remember that many of the EDL models consider the electrode surface not as a porous material but as a flat plane. Furthermore, the gas molecule used (generally nitrogen) to probe the pore volume and the electrolyte ions displays different size and interaction with the material surface. Therefore, the approximately

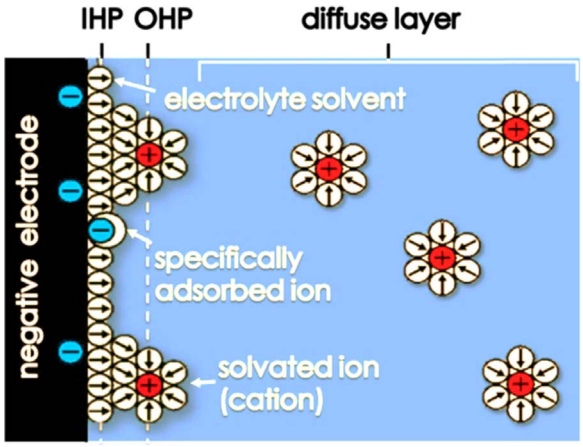

Fig. 1. Schematic representation of the BMD double-layer model on a negatively polarized electrode (based on Ref. [33]).

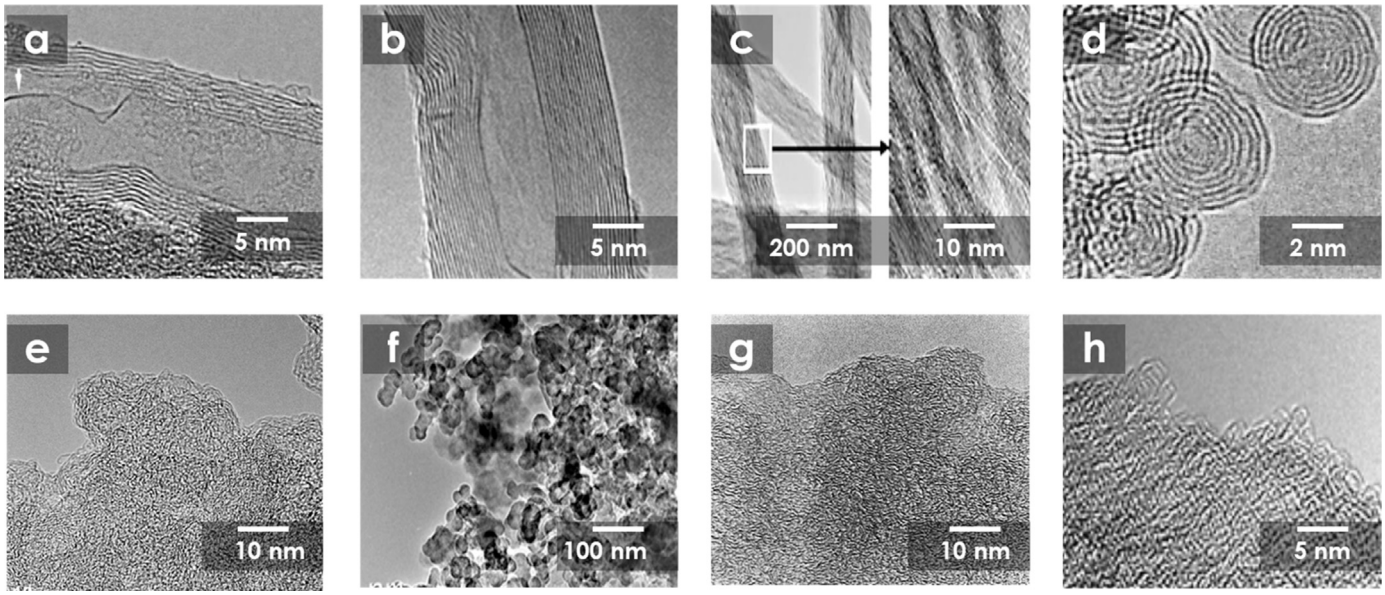

Fig. 2. Transmission electron micrographs of various carbon nanomaterials used for capacitive applications: (a) multi-layer graphene nanoribbon [89]. (b) Multi-walled carbon nanotube (MWCNT) [90]. (c) Carbon nanofibers from aligned electrospun polyacrylonitrile (PAN) [91]. (d) Carbon onions [92]. (e) Carbon black produced by incomplete combustion of heavy petroleum products [93]. (f) Carbon black [69]. (g) Activated carbon (AC) from coconut shells [94]. (h) Carbide derived carbon (CDC) from PMMA templates [88].

estimated specific surface area of porous electrodes evaluated by gas adsorption, which is generally different from the active surface area which takes part in EDL charging, cannot be directly considered for the specific capacitance calculations.

3. Carbon electrode materials for capacitive applications

The performance of capacitive technologies is highly dependent on the device design and operation parameters. Owing to a wide range of allotropes, tunable and adjustable structure of nanopores, and controllability of surface functionalities, carbons are the most frequently used electrode materials for capacitive applications [35]. In addition, the low atomic number qualifies carbon as a lightweight material; thus, carbon-based systems are often characterized by high performance normalized to mass (i.e. gravimetric capacitance). From the point of view of economic and ecological aspects, the high natural abundance of organic precursors and possibility to utilize renewable sources (i.e. food wastes, agricultural residues) for manufacturing of electrodes are the additional advantages of carbon materials [36–39].

An overview of several carbons applied for capacitive technologies is presented in Fig. 2. A basic structural component of many carbon allotropes, such as graphite, charcoal, and carbon nanotubes is graphene. Graphene is a 2-D structured carbon material which exhibits a flake-like shape (Fig. 2a) and, in theory, can provide specific surface area of ca. 2630 $m^2 g^{-1}$, yet in practice it is often below 500 $m^2 g^{-1}$ for graphene electrodes [40,41]. Graphene-based electrode materials can be prepared with different macrostructural complexity, from free-standing particles or dots, through fibers, yarn and films, to foams and composites [42,43]. There has been a lot of attention given to the multilayer graphene films on account of their tunable thickness, structural flexibility, lightweight and electrical properties which fulfill the essential qualities required for capacitive technologies employing flexible devices [44]; besides, the high conductivity of graphene sheets enables a low diffusion resistance, thus leading to enhanced power and energy density [45,46]. Many research efforts have been dedicated to exploring novel processing methods to obtain graphene-based films, such as spin-coating, layer-by-layer deposition, vacuum filtration, and interfacial self-assembly [47,48]. A critical issue entailing the decrease of accessible surface area and reduction of ions diffusion rate is agglomeration and restacking due to the strong π-π interactions between the layers. Numerous attempts have been undertaken to break this processing bottleneck, by using template-assisted growth of the sheets or adding spacers between the graphene layers. Nevertheless, incorporating guest nanoparticles into multilayered graphene also limits the access of ions to the active surface on the graphene planes, even if the bridges favor the reduction of graphene sheets aggregation [49]. In this context, graphene-based macrostructures with 3-D networks, i.e., aerogels, graphene foams and sponges caught a recent attention of researches interested in technologies dedicated to energy storage, deionization and catalysis. The interconnected pores of various size provide fast ion transport channels and relatively high surface area, which are highly desirable for exploring high power and energy density, and overall high capacitive performance. Recently, free-standing holey graphene frameworks (HGF), also called graphene nanomesh, with efficient ion transport pathways were reported [50]. HGF can be prepared through hydrothermal reduction of graphite oxide (GO) with simultaneous etching of graphene at around 200 °C, owing to the presence of H_2O_2 molecules. Due to the formation of nanopores in the graphene sheets, this 3-D self-assembled structure enables to reach high capacitance values (298 $F g^{-1}$ at 1 $A g^{-1}$) in 1-ethyl-3-methylimidazolium tetra-fluoroborate/acetonitrile ($EMIMBF_4$/ACN). Nevertheless, one has to realize that HGF is formed by removing a large number of carbon atoms from graphitic planes, which actually results in a material quite far from intact graphene.

When graphene is rolled-up to tubular 1-D nanostructures, single wall (SWCNTs) or multi-walled carbon nanotubes (MWCNTs) are created, containing either one or several graphene sheets, respectively (Fig. 2b) [51]. Owing to their good mechanical and electrical properties (conductivity ~ 5000 $S cm^{-1}$) [52,53], CNTs have been widely investigated as electrode materials especially to enhance the power density in electrochemical capacitors [54]. Carbon nanotubes are generally produced by catalyst assisted chemical vapor deposition (CCVD) using a hydrocarbon feedstock, such as methane, acetylene and propylene [55], creating cylinders which extend around hundreds of μm in the axial direction [56]. Plasma etching is sometimes employed to properly open the top end-caps of CNTs and allow the electrolyte access to their otherwise inaccessible inner cavity [57]. Electrophoretic deposition (EPD) has been explored for placing formerly grown CNTs onto a metal current collector and to reduce the contact resistance. As a result, impedance spectroscopy measurements on EDLCs using carbon nano-

tubes mats as electrodes deposited on nickel foil current collectors in 6 moL L^{-1} KOH electrolyte reveal low equivalent series resistance (ESR) (0.75 Ω) and relatively high value of so-called knee frequency (the transition point between the high-frequency component (inclined at 45°) and the low-frequency component (near vertical) region) [58]. The reported knee frequency of around 7.6 kHz, compared to the values for capacitors with CNT electrodes which are generally much lower than 0.1 Hz, demonstrates the improved power capabilities of EDLCs using carbon nanotubes films deposited by electrophoretic deposition. In order to produce much thicker carbon fibers than CNTs, alternative methods, such as electrospinning of polyacrylonitrile (PAN, Fig. 2c) followed by carbonization, were introduced. Depending on the synthesis conditions and thermal treatment procedure, carbon fibers from PAN are characterized by a variable degree of carbon ordering [59,60].

Capacitive nanomaterials can be also found among quasi 0-dimensional (0-D) carbon particles. Whereas buckminster fullerites themselves are not attractive for capacitive applications because of their semiconductive nature [61], carbon onions, also called carbon nano-onions (CNOs) or onion-like carbons (OLCs), which contain concentric spherical carbon shells (Fig. 2d) of fullerene-like or polyhedral nanostructure have been explored for capacitive technologies [62]. Carbon onions are commonly synthesized by few-step graphitization of nanodiamonds at very high temperatures (> 1700 °C) in inert atmosphere or under vacuum [63]. The specific surface area of the resulting CNOs (up to 400–600 m^2 g^{-1}) is fully accessible to ions [64], whereas their nanoscopic size (< 10 nm in diameter) and 0-D structure enable easy dispersion, as compared to 1-D nanotubes and 2-D graphene [65]. However, due to their high cost and low capacitance (around 50 F g^{-1} in H_2SO_4 and 40 F g^{-1} in Et_4N-BF_4/ACN) [64,66] resulting from low specific surface area, CNOs are rather used as conductive additive to carbon based electrodes than primary active material for high-power EDLCs.

If one is interested in a high surface area material while keeping the spherical shape, carbon black (CB) produced by incomplete combustion of heavy petroleum products (fluid catalytic cracking (FCC) tar, ethylene cracking tar or coal tar) offers even more than 1500 m^2 g^{-1} [67,68]. The porosity in this case is due to the agglomeration of nanoparticles with size ranging from 10 to 50 nm (Fig. 2e), creating an external SSA which is much larger than the value typically revealed by CB (below 100 m^2 g^{-1}) consisting of multi-walled carbon spheres in necklace-like arrangement (Fig. 2f) [69]; yet, the agglomeration of small particles in chains results in good electrical conductivity of the latter CB which is often used as additive to carbons with non-ordered nanostructure.

The by far most commonly used type of carbon material for capacitive technologies is particulate and nanoporous activated carbon (AC), which can be recognized as a complex and disordered agglomeration of nano-scale units (Fig. 2g) [6]. The units are constituted of graphene layers randomly oriented and strongly cross-linked, impeding the movement of the layers to a more parallel arrangement [70], and sometimes involve single fragments of curved and faceted graphene layers connected with each other [71,72]. Activated carbons are the most commonly used materials for capacitive applications, owing essentially to their low cost, versatility of porous texture, high conductivity and high specific capacitance [6]. Generally, ACs have specific surface area of 1500–2000 m^2 g^{-1}; however, many activated carbons have lower SSA, yet their amount of micropores allows high capacitance to be obtained [67]. The final properties of ACs are strongly influenced by the nature of precursors and conditions of the activation process, and whether'so-called' chemical or physical removal of carbon is employed. The common natural organic precursors for activated carbon synthesis include: coal, peat, fruit stones, nut shells, wood, petroleum coke, pitch, lignite, starch, sucrose, corn grain, leaves, coffee grounds, straw etc [73,74]. In general, carbonized samples from natural organic precursors have a relatively low porosity with a large number of interstices which block the pore entrances. Therefore, the pre-carbonized products must be further physically or chemically activated in order to open the porosity and to create new pores. Physical activation is conducted by gasification of pre-carbonized chars at temperatures ranging from 700 to 1000 °C, in the presence of an oxidizing gas (such as CO_2, steam, air or a mixture of these gases), which increases the pore volume and surface area of the material by a controlled carbon burn-off. The production of ACs by chemical activation, carried out at slightly lower temperatures (~ 400–700 °C), involves the reaction of a precursor or a char with a chemical reagent (such as KOH, $ZnCl_2$ or H_3PO_4) [75–77]. As reported, by activation with potassium hydroxide, it is possible to obtain ACs with BET specific surface area up to 3500 m^2 g^{-1} [78]. Nonetheless, to remove the residual reactants as well as any inorganic residues (e.g., ash) which originate from the carbon precursor or are introduced during preparation, post-activation washing is always required. Although it is generally believed that the activation process is required to open the pores of carbonized precursors, carbons with well-developed porosity and good capacitance values, as well as reproducible properties can be also obtained by simple one-step carbonization of synthetic polymers, e.g., through a rapid microwave heating of polypyrrole (PPy) [79,80]. Recently, it has been also presented that self-activation can proceed during the carbonization of appropriate biomass precursors, e.g., tobacco [38] or seaweeds [81,82], where the second stage of chemical or physical activation is unnecessary. Owing to the presence of naturally embedded group I and II elements (such as potassium, calcium, magnesium, sodium), carbonization and self-activation of the precursor occur simultaneously during the thermal treatment.

Another form of nanoporous carbon particles, namely carbide-derived carbons (CDCs), is synthesized by dry chlorine treatment of non-organic precursors, such as carbides and carbonitrides [83]. CDCs appear as attractive materials for capacitive technologies, when high S_{BET} (up to 3100 m^2 g^{-1}) is researched [84,85]. For tailoring CDCs with ordered pore architectures, soft- or hard-templating methods are employed with using amphiphilic structure-directing agents or solid-state templates, respectively [86,87]. However, if one does not want to deal with organic solvents and surfactants, or avoid the additional synthesis steps for template removal, other alternatives for formation of micro- and mesoporous templated carbons can be proposed. For instance, CDCs can be tailored by applying a templating method based on the simultaneous thermal decomposition of poly(methyl methacrylate) (PMMA) (the pore forming material) and conversion of a polycarbosilane polymer precursor into silicon carbide, followed by silicon elimination under chlorine gas at high temperature (Fig. 2h) [88].

Many review articles discuss the particular issue of ensuring low cost of carbon materials for charge storage-based technologies while keeping high capacitance/capacity per unit volume or mass [4,6–13,41,95–97]. To find the most proper carbon material for a certain capacitive application, it is important to thoroughly review the set of specific requirements. For example, if one is interested in improving the ion transport rate, materials with a large external surface area (such as graphene or carbon onions) should be preferred to provide a transport pathway [95]. When considering energy efficient water desalination with flowable carbon suspension electrodes, the particle shape, viscosity, and agglomeration behavior become key factors to consider [98].

An important aspect for an appropriate selection of carbons for capacitive applications is closely connected with the porous texture (specific surface area, pore volume, size and shape of pores, tortuosity). A high porosity is beneficial, and the pores must be large enough to accommodate ions (at least in the desolvated state for electrolyte systems employing solvents, or along the short axis for solvent-free ionic liquids). According to the IUPAC classification, there are three main kinds of pores: (i) micropores (with diameter < 2 nm), mesopores (diameter from 2 to 50 nm) and macropore (diameters > 50 nm) [99]. It was already shown that the micropores accommodate more ions

[100,101], while the mesopores do not take part in the actual adsorption processes, but allow the ions to be transported to the micropores [102–104].

Adsorption of a gaseous medium (most commonly nitrogen) at a fixed temperature (N_2: −196 °C, CO_2: 0 °C) is the most frequently employed method to investigate the porosity of carbon electrodes. Their porous characteristics are estimated from the adsorption (or desorption) isotherm, using a model of the sorption process [105–107]. In highly porous electrodes, adsorption may occur via a pore filling mechanism rather than by the surface coverage only (as it is assumed by the Langmuir and Brunauer-Emmett-Teller theory (BET) [108]). In such cases, the application of the BET equation can lead to unrealistically high surface-area (S_{BET}) estimations. Furthermore, many authors in the literature assume that the surface area of the electrode/electrolyte interface in Eq. (1) is equivalent to the BET surface area of the electrode material, and thereby overestimate the values of gravimetric capacitance in the narrow pores (see also Section 4.1) [109,110]. More and more often, the regularized density functional theory (DFT) is taken into consideration as a more accurate way to correlate capacitance with specific surface area (SSA). In this model, adsorption and capillary condensation in pores of slit-shaped geometry (or other geometries, like mixed slit/cylindrical) is assumed [111]. More advanced approaches even consider the complementary information from sorption isotherms of different gases (e.g., CO_2 and N_2) combined with 2D-NLDFT models.

Fig. 3 shows that the gravimetric capacitance of a series of activated carbons (ACs) and carbon blacks increases almost linearly with the BET specific surface area up to ≈ 1500 m^2 g^{-1}, and then for carbons with higher activation degree a plateau connected with porosity saturation is visible [112]. For the same carbons, the proportionality region of capacitance with S_{DFT} is more extended than when using S_{BET}, but still for S_{DFT} higher than 1200 m^2 g^{-1} saturation can be observed (Fig. 3). The saturation of capacitance is associated with the decrease of pore wall thickness due to the increase in activation degree [112]. When approaching the screening length of the electric field (δ_{SC}), the adjacent space charge regions in the pores start to overlap, which basically leads to incomplete charge screening. It is important to remember that the capacitive performance is not only the consequence of particles porosity, but also electrode architecture and film thickness. The fast ion transport optimization enabled by using nanometer-sized carbon particles [113], very thin electrodes of micrometer-sized carbon particles [114] or carbons with hierarchical porous structure [115], also has an important impact on ions electrosorption.

Carbon may also be used as secondary phase, e.g., to serve as conductive additive in order to enhance the charge distribution efficiency through the electrode material. Unless the specific capacitance of the additive is equal or even higher than that of the active carbon electrode material, a deterioration of the composite electrode performance is always observed after admixing any conductive additive [67]. This statement relates to the equilibrium capacitance (the double-layer capacitance at low scan rate or low current density) and reflects the numeric decrease in specific pore volume and specific surface area available for storing the electrosorbed ions.

Improving carbon conductivity on a particle-level is another strategy to enhance the electrochemical performance [116,117]. Thus, doping carbons with heteroatoms, such as nitrogen, boron, sulfur, or phosphorous has been extensively studied [118–120]. However, it is important to note that a decreased electrical conductivity was also found for some carbon nanotubes after doping with nitrogen [121]. Additionally, the interaction of ions with doped carbon surfaces may lead to enhanced double-layer capacitance [122], and redox-active surface sites [123] may also appear and be used for enhanced energy storage and recovery beyond capacitive ion electrosorption processes. There are nevertheless examples where a high amount of electrochemically active heteroatoms may severely lower the salt removal capacity efficiency for CDI [124]. Therefore, it is always important to balance the requirement for a certain capacitive application, bearing in mind that the high capacitance/capacity per unit volume or mass is a crucial, but not only issue. More information about specific details and guidelines for selecting preferable carbon materials for a certain technology will be provided in the following sections.

4. Electrical double-layer capacitors (EDLC)

4.1. Introduction

Contrary to conventional capacitors (such as electrolytic capacitors) which contain a dielectric material sandwiched between two electrodes facing each other, electrical double-layer capacitors (EDLCs) use the electrical double-layer to accomplish nanoscale charge separation [14,15]. In general, EDLCs are made from two identical porous carbon electrodes separated by a membrane soaked with the electrolyte. When the device is connected to a power supply, an equal amount of positive and negative charges is distributed between the positive and negative electrodes (Fig. 4). Therefore, the device is equivalent to two capacitors of capacitance C_+ and C_- and resistance R_{f+} and R_{f-} in series Due to this series arrangement, the capacitance C of the device is given by Eq. (5):

$$\frac{1}{C} = \frac{1}{C_+} + \frac{1}{C_-} \tag{5}$$

Since the capacitance of the two carbon electrodes is generally different (even in a symmetric capacitor), according to Eq. (5), the

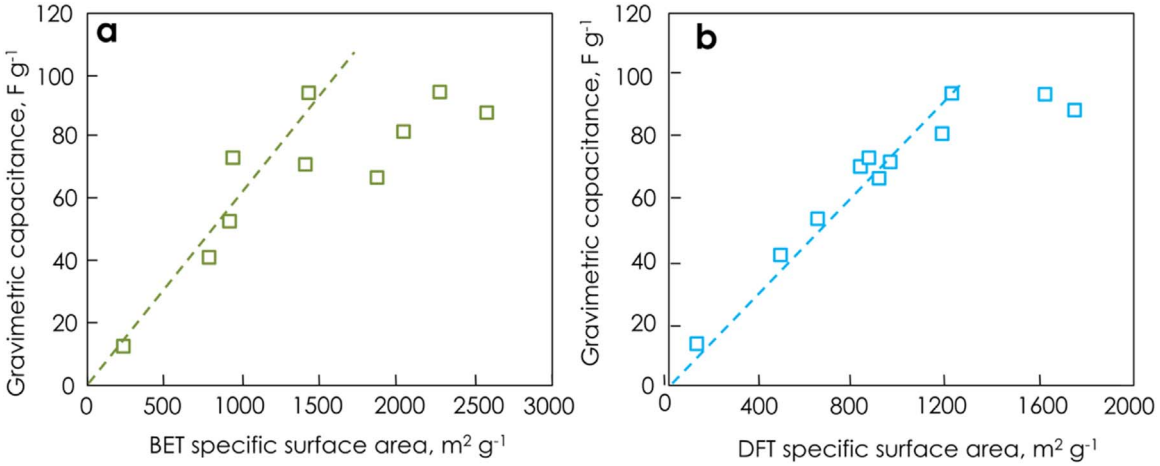

Fig. 3. Gravimetric capacitance *vs* (a) BET and (b) DFT specific surface area of a series of ACs and carbon blacks (adapted from [112]).

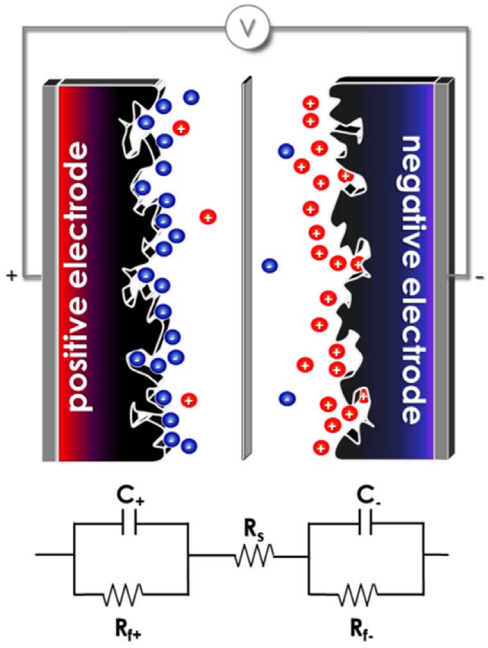

Fig. 4. Schematic representation of the charged state of a symmetric electrical double-layer capacitor using porous carbon electrodes and its simplified equivalent circuit (adapted from [6]).

capacitance of the device is determined by the electrode with the smallest capacitance.

The key feature of EDLCs and any capacitive system is a linear capacitor-like correlation between voltage and charge, which is in contrast to battery-like systems. The capacitor-like behavior can be maintained even when faradaic processes (i.e., redox reactions) occur, and it is generally referred to as pseudocapacitance [125,126].

In order to determine the capacitance of the system, galvanostatic charge/discharge (GCPL) is usually performed, with measuring the voltage variation as a function of time. For an ideal EDLC, the cell capacitance is expressed by formula (6):

$$C_{cell} = \frac{I\Delta t}{\Delta U} \quad (6)$$

where I is the applied current (A), Δt – the discharge or charge time (s) and ΔU is the change in voltage (V) corrected from the Ohmic drop. When the profile of galvanostatic discharge deviates from linearity, the capacitance has to be calculated from the total stored energy [127,128].

If both electrodes display comparable capacitance, formula (7) can be applied to calculate the specific capacitance (F g^{-1}) of a single electrode:

$$C_{el} = \frac{2C_{cell}}{0.5m_{el}} \quad (7)$$

where m_{el} is the total mass of electrodes (g).

Since the charge storage in EDLCs is based on ions electrosorption inside the pores, the textural properties of electrodes have a very high impact on the capacitive performance of these devices. Therefore, in order to better understand the behaviour of ions in the porosity of carbons and to design proper electrode materials for EDLCs, electrolytes with a well-defined ion size such as ILs are generally used to analyse the mechanism of charge storage. However, even if carbon materials with well-tailored pores are applied, the charge accommodation in the porosity of the two electrodes may occur differently than assumed, due to different size of cations and anions and eventual addition of solvent for improving the transport properties. Therefore, studies attempting to reveal the different charge storage mechanisms of the neat/solvated ions in carbon/carbon EDLCs will be presented in the following section.

4.2. Charge storage mechanisms in EDLCs with porous carbon electrodes

The EDL composition and rearrangement of electrolyte species on the electrode surface under polarization is different for nanoporous carbon electrodes and for flat metal plates. As already mentioned in Section 3, the surface area of the electrode/electrolyte interface in Eq. (1) cannot be substituted by the BET specific surface area (S_{BET}) calculated from nitrogen adsorption at −196 °C [129,130], where adsorption may occur not only via surface coverage but also by pore filling mechanism. In addition, the nitrogen probe has a different size as compared to electrolytes ions, and the driving forces are different for nitrogen adsorption and ions electrosorption. Moreover, it has been demonstrated that the claimed increase of normalized capacitance (capacitance divided by specific surface area) in pores smaller than 1 nm versus average micropore size L_0 for TiC-derived carbons using tetraethylammonium tetrafluoroborate in acetonitrile (Et_4N-BF_4/ACN) [131], depends on the model used for determining the specific surface area [132]. Indeed, S_{BET} was compared with the average surface area S_{av} of 42 microporous carbons (including carbide-based carbons and monoliths to exclude any blurring of the binder in the determination of S_{av}) with L_0 between 0.66 and 1.65 nm [132]. S_{av} was calculated by combining the Dubinin-Radushkevich equation (S_{DR}) [133], the density functional theory (S_{DFT}), the Kaneko's comparison plot on nitrogen adsorption isotherms at −196 °C (S_{comp}) [134,135] and phenol immersion enthalpy (S_{phenol}) [136,137]. The comparison revealed that S_{BET} and S_{av} are similar to each other only for pores width of ~ 0.9 nm; for pores broader than 0.9 nm, the specific surface area of carbons is overestimated by the BET model, whereas it is underestimated for pores narrower than 0.9 nm. As a consequence, C/S_{BET} increases when L_0 decreases (Fig. 5a), as already claimed in Ref. [131], reaching an outstanding value of 0.15 F m^{-2} at L_0 = 0.7 nm. However, when the capacitance is normalized by using $S_{>0.63\ nm} = S_{tot} - S_{<0.63}$, where S_{tot} is the average value of S_{DR}, S_{comp} and S_{phenol}, and $S_{<0.63}$ is the surface inaccessible for the oblate spheroidal Et_4N^+ desolvated cation with equatorial diameter of 0.63 nm [138] (instead of the polar diameter of 0.67 nm [139] generally considered for Et_4N^+), the normalized capacitance $C/S_{>0.63\ nm}$ does not depend significantly on the average micropore size L_0 (Fig. 5b).

Even if the aforementioned debate clearly illustrates that inappropriate data manipulation can lead to contradictory conclusions regarding normalized capacitance, it should not hide more important information. Indeed, considering the diameter of ACN-solvated Et_4N^+ (1.3 nm) and BF_4^- (1.16 nm) and the striking high capacitance values observed with carbons having 0.7–0.8 nm pores diameter closer to the size of desolvated Et_4N^+ (0.67 nm) and BF_4^- (0.48 nm) [139], Vix-Guterl et al. have been the first to suggest that, under electric polarization, ions are at least partly desolvated in micropores [4]. Later, desolvation of ions has been directly confirmed by nuclear magnetic resonance (NMR) on AC electrodes extracted from capacitors charged up to different voltage values in the Et_4N-BF_4/ACN electrolyte. The molar proportions of Et_4N^+ (n_{Et4N} / $n_{Et4N}+n_{BF4}$) and BF_4^- (n_{BF4} / $n_{Et4N}+n_{BF4}$) and the relative amount of ACN vs. total amount of electrolyte species (n_{ACN} / $n_{ACN}+n_{Et4N}+n_{BF4}$) in the two electrodes after polarization at various voltages are shown in Fig. 6 [141]. Owing to charging, the Et_4N^+ cations in the positive electrode are replaced by BF_4^- anions, while the amount of solvent molecules remains nearly constant up to 4.0 V. Simultaneously, in the negative electrode, small anions are replaced by larger cations, while the ACN concentration decreases and becomes negligible at 2.7 V (i.e., no ACN molecules are left in the micropores of the AC-based electrode). So, it can be clearly seen that the solvent has an important responsibility in the composition of the EDL and in its further instabilities when applying low cathodic or high anodic polarization.

To provide a detailed view on the storage mechanisms Fig. 7a presents in-pore ions population determined by *in-situ* NMR at

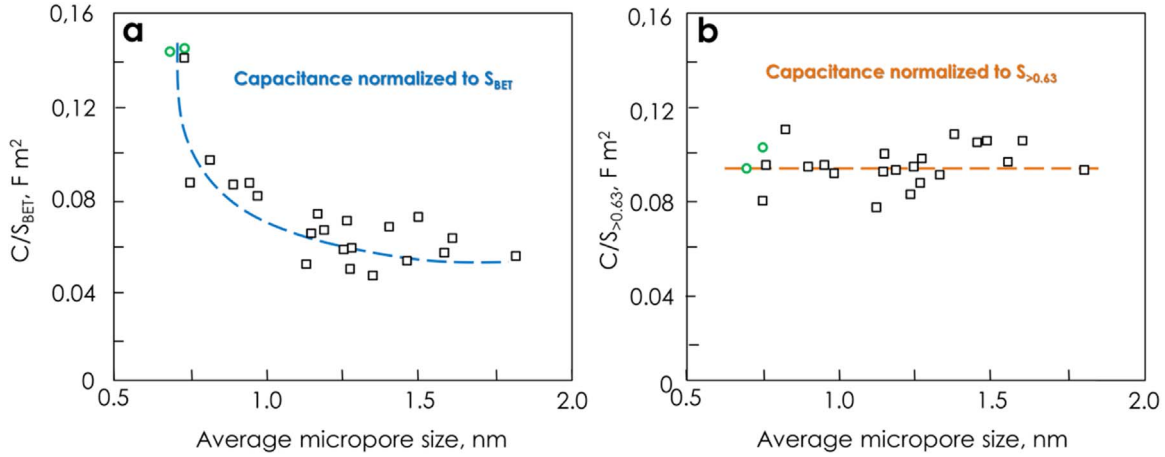

Fig. 5. Variation of normalized capacitance in Et_4N-BF_4/ACN *vs* average micropore size for a variety of porous carbons (black squares) and carbon monoliths (green circles) with pore widths around 0.7 nm: (a) normalized to BET specific surface area; (b) normalized to $S_{>0.63\ nm} = S_{tot} - S_{<0.63}$ specific surface area (S_{tot} is the average value of S_{DR}, S_{comp} and S_{phenol}; $S_{<0.63}$ is the surface area of micropores in the ranges 0.33–0.41 and 0.41–0.63 nm obtained by N_2 adsorption and immersion enthalpy calorimetry, respectively) (adapted from [140]).

different charged states of a single activated carbon electrode (YP50F) in 1.5 mol L^{-1} PEt_4-BF_4/ACN [142]. When the electrode is positively polarized (from 0 to 1.5 V vs. carbon), charging occurs essentially by ion-exchange (counter-ion adsorption accompanied by simultaneous co-ion desorption from the pores, where counter-ions and co-ions are defined as having charge with opposite and same sign as the electrode, respectively) [143–145]. In contrast, when the electrode is negatively charged (from 0 to −1.5 V vs. carbon), the anions population inside the micropores does not change, while the cations continue to be accommodated (so called perm-selective cation adsorption). Interestingly, the same phenomenon was observed for different electrolyte concentrations (1.5, 0.75 and 0.5 mol L^{-1} PEt_4-BF_4 in ACN) [142], suggesting that the amount of solvent does not dictate the charging mechanism, but that solvent species only accompany the adsorbed ions.

Variation in compositional changes inside the electrode depending on the amount of stored charge can be also investigated by *in-situ* electrochemical quartz crystal microbalance (EQCM) based on analysing the electrode mass change per unit area when a constant potential sweep is applied [146,147]. The obtained results are usually compared with the theoretical mass change calculated from Faraday's law when adsorption of neat counter-ions takes place. EQCM studies on a CDC electrode in 2 mol L^{-1} 1-ethyl-3-methylimidazolium bis(trifluoromethanesulfonyl)imide in acetonitrile (EMI-TFSI/ACN) electrolyte have shown the much greater than expected mass change of the negative electrode (domain I in Fig. 7b) [146]. Since anions are left in the pores of the negative carbon electrode, the total electronic charge is balanced by an excess of cations via the perm-selective counter-ion adsorption, as revealed by NMR (Fig. 7a) [142]. When the electrode is positively polarized (domain II), the measured electrode mass change is smaller than the theoretical mass expected for pure counter-ion adsorption, indicating an ion-exchange [146,148], i.e. the slightly heavier cations (EMI^+) are desorbed from the pores of the positive electrode, while the lighter anions ($TFSI^-$) are adsorbed. For charge densities larger than 0.001 C cm^{-2}, the counter-ion adsorption mechanism is dominant and the mass of the positively charged electrode starts to increase. For the high charge densities (domain III), the slope of the measured mass change becomes parallel to the theoretical one, owing to pure counter-ion adsorption.

The different charging mechanisms for negative and positive polarization can be also revealed by analyzing the increase of electrodes volume, using electrochemical dilatometry [149,150]. Fig. 8 shows the dimensional changes of a carbon black (BP2000) electrode in 1-ethyl-3-methyl-imidazolium tetrafluoroborate (EMI-BF_4), with and without ACN, during positive (0 to 1.7 V vs. carbon) and negative polarization (0 to −2.0 V vs. carbon) by cyclic voltammetry (Fig. 8a and b) [151]. The larger relative dilatation observed in Fig. 8c and d for negative polarization than for positive one confirms that additional species are accommodated during charging under negative polarization.

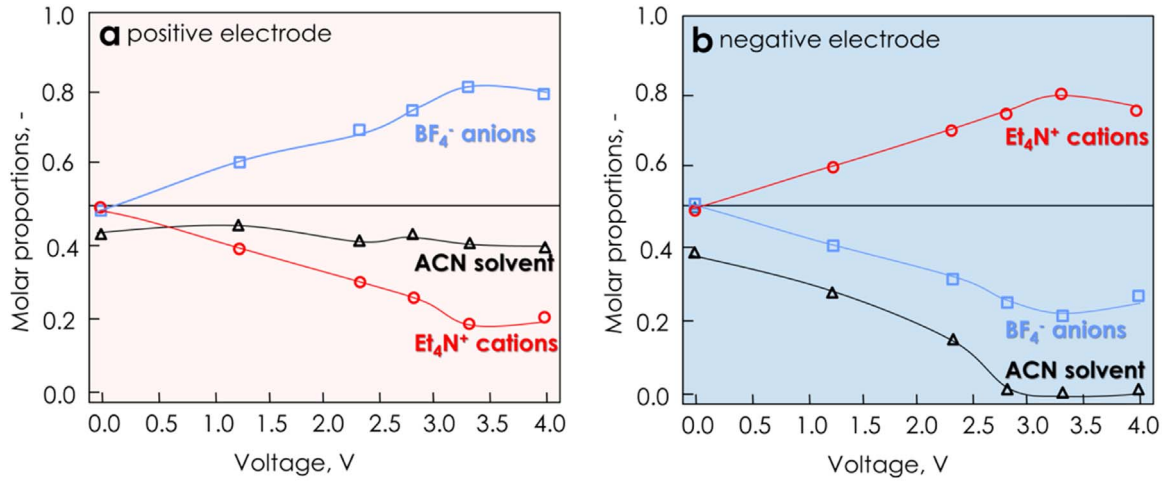

Fig. 6. Molar proportions of Et_4N^+ (n_{Et4N} / n_{Et4N}+n_{BF4}) and BF_4^- (n_{BF4} / n_{Et4N}+n_{BF4}) and the relative amount of ACN (observed after drying, therefore adsorbed or solvating) vs. total amount of electrolyte species (n_{ACN} / n_{ACN}+n_{Et4N}+n_{BF4}) in (a) positive electrode and (b) negative electrode calculated from NMR spectra recorded after polarization of a symmetric carbon/carbon EDLC at various voltages for 30 min (adapted from [141]).

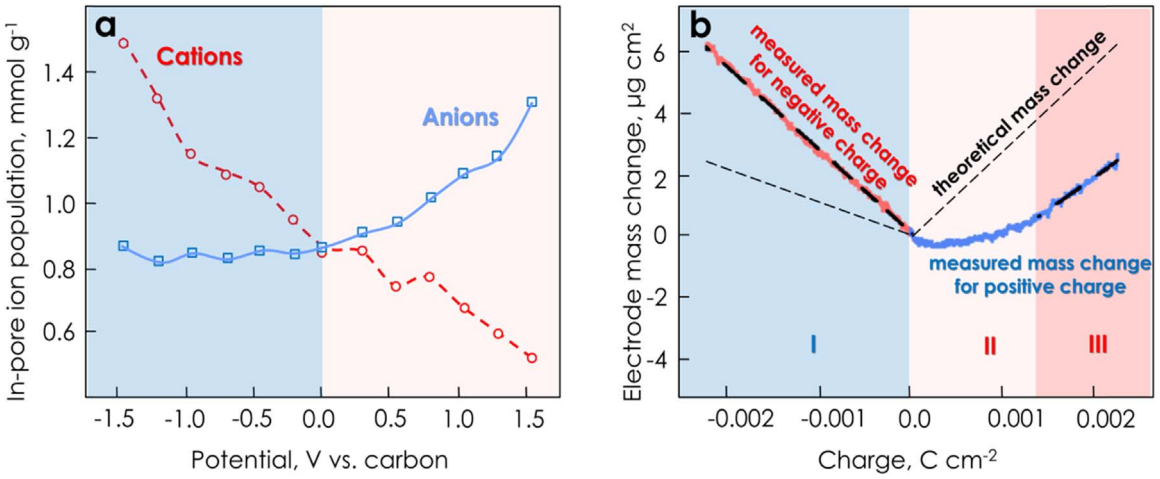

Fig. 7. (a) In-pore ions population per gram of single activated carbon electrode (YP50F) in 1.5 mol L^{-1} PEt_4-BF_4/ACN at different charged states of the electrode determined from the deconvoluted NMR intensities (adapted from Ref. [142]). (b) Electrode mass change vs charge measured by EQCM during polarization of carbide-derived carbon with 1 nm average pores size (CDC-1nm) in 2 mol L^{-1}1-ethyl-3-methylimidazolium bis(trifluoromethanesulfonyl)imide in acetonitrile (EMI-TFSI/ACN) (adapted from Ref. [146]).

Nevertheless, the impact of different size of cations and anions on dilatation of polarized electrodes should not be neglected. It is also interesting to remark that, during negative charging, the relative strain increases from 3.4% to 4.2% after adding ACN to the ionic liquid, while solvent addition almost does not affect the dimensional changes for the positive electrode (expansion from 0.8% to 1.0%) (Fig. 8c and d) [151]. It suggests that the additional mass changes appearing especially for the negative electrode (as observed in Fig. 7b) are not only attributed to additional ions which accommodate in the electrodes pores but also to some solvent molecules accompanying the adsorbing ions.

The strong change in the ratio of cations and anions in the pores of electrodes has also a significant influence on the thermo-physical behavior of ionic liquids in the pores. The low temperature electrochemical studies in three-electrode cell (working electrode (WE), counter electrode (CE) and carbon reference electrode) performed by polarizing the WE positively (up to around 0.2 V vs carbon reference) and negatively (down to around −0.2 V vs carbon reference) and monitoring the CE potential vs reference, revealed different freezing

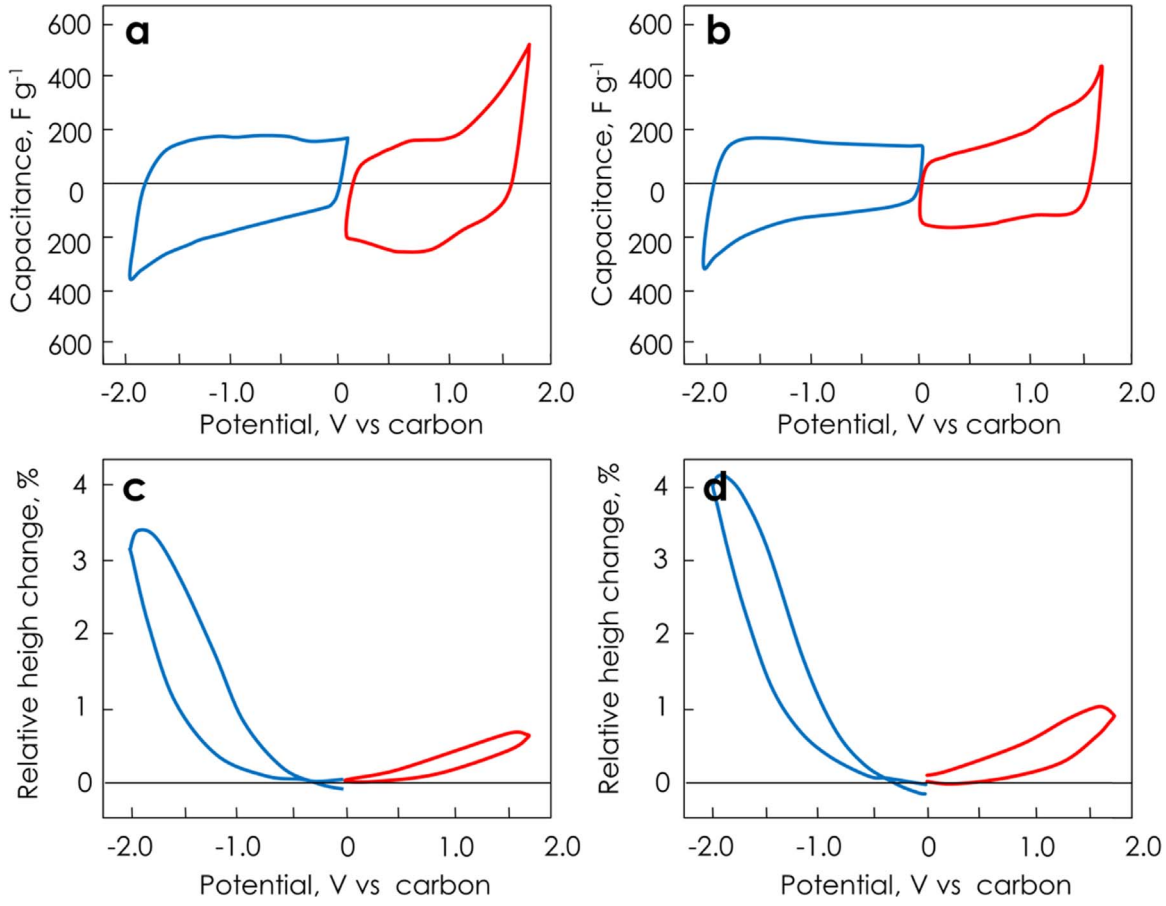

Fig. 8. (a, b) Cyclic voltammograms (1 mV s^{-1}) of a carbon black (BP2000) electrode in EMI-BF_4 with (right) and without (left) acetonitrile; (c, d) Respective relative electrode expansion [151].

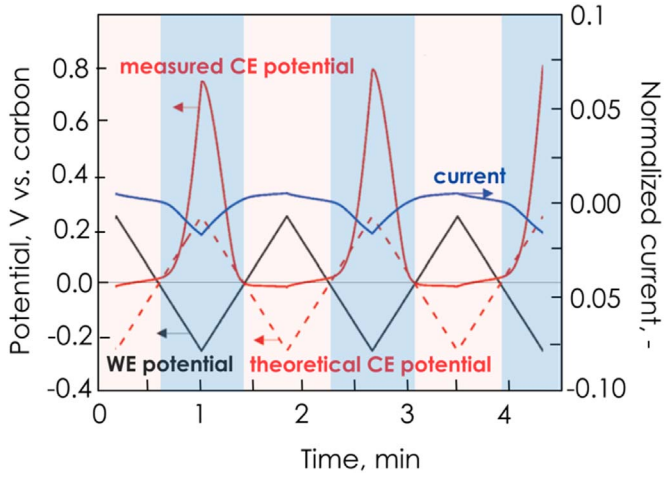

Fig. 9. Imposed working electrode (WE) potential, theoretical and measured counter electrode (CE) potential, and current evolution during cycling at 10 mV s^{-1} of a carbon black (BP2000) working electrode in 10 wt% BMI-BF_4 in EMI-BF_4 at −20 °C (adapted from Ref. [152]).

and thawing of a mixture of 1-butyl-3-methyl and 1-ethyl-3-methyl imidazolium tetrafluoroborate (10 wt% BMI-BF_4 in EMI-BF_4) in the two carbon electrodes [152]. The asymmetric profile of current signal observed during cycling at −20 °C (Fig. 9) is probably the result of vast differences in the anions and cations mobility. Furthermore, it can be seen that when the WE is negatively polarized (blue region in Fig. 9), the anions are still mobile at −20 °C being adsorbed in the pores of the positive electrode (observed as an increase of the measured CE potential). When the WE is positively polarized (red region in Fig. 9), the steric effects of cations and the overall high viscosity of the electrolyte at low temperature result in much lower measured CE potential than the theoretical one exhibited for an ideal EDLC. It is noteworthy that the crystallization of EMI-BF_4 is partially hindered in the applied conditions by adding BMI-BF_4 with a long cation alkyl chain [153].

To improve the power performance of IL-based EDLCs at low temperatures, binary mixtures of ionic liquids can be applied to reduce the melting temperature. For example, a mixture of N-methyl-N-propylpiperidinium bis(fluorosulfonyl)imide (PIP_{13}-FSI) and N-butyl-N-methylpyrrolidinium bis(fluorosulfonyl)imide (PYR_{14}-FSI) in 0.5:0.5 M ratio enables to extent the liquid state of the electrolyte down to −80 °C, whereas the melting points of the separate constituents are 6 °C and −18 °C for PIP_{13}-FSI and PYR_{14}-FSI, respectively [154]. Besides, a proper design of the carbon electrode, where e.g., the EDL is formed on the outer surface of carbon nanoparticles can reduce the ion transfer limitations at low temperatures. On the way of combining these two strategies, the application of binder-free electrodes made of vertically aligned carbon nanotubes (VA-CNTs) enables an EDLC with the $(PIP_{13}\text{-FSI})_{0.5}(PYR_{14}\text{-FSI})_{0.5}$ mixture to operate in the temperature range from −50 °C to +100 °C [155]. Owing to the large intertube distance which enhances the electrochemical accessibility of the electrolyte to the VA-CNTs surface, the capacitance value ($C/C_{20\ °C}$) at −50 °C is close to 1 while applying a potential scan rate of 5 mV s^{-1}. Once again, these results emphasize the importance of a proper design of the carbon electrode architecture in conjunction with the electrolyte formulation for extending the operating range of EDLCs and adapting these devices for specific applications under extreme climatic conditions.

Since a careful selection of the electrolytic solution is also important when considering the possible operating voltage and capacitance properties of EDLCs, the following paragraphs will introduce studies revealing that trapping of electrolytic species from aqueous solutions in the porosity of negative AC electrodes results in, e.g., pH variations, and reaching larger electrochemical window than for the standard water-based electrolytes. Furthermore, reactions involving redox-active electrolyte species such as hydroquinone/p-benzoquinone (HQ/BQ) or iodide/iodine ($2I^-/I_2$) couples at the surface of positive AC electrodes will be presented as an interesting option to increase capacitance and consequently the energy density.

4.3. Hydrogen electrosorption in the pores of the negative electrode

In recent years, the number of researches on electrochemical capacitors (ECs) in aqueous electrolytes has tremendously increased, as the systems based on these media are much more environmentally friendly than EDLCs employing organic solvents and can be produced at very low cost. Indeed, while implementing non-aqueous electrolytes, all components (carbon material, separator, electrolyte itself) need to be well-dried and assembled in moisture free atmosphere in order to ensure a long life span of the system, whereas drying is not required in case of aqueous electrolytes, enabling the cost of the final device to be dramatically lowered [156]. However, when considering the formula of the usable energy E:

$$E = \frac{1}{2} C_{cell} U^2 \tag{8}$$

where C_{cell} is the cell capacitance (F g^{-1}) (as calculated from Eq. (6)) and U is the operating voltage (V), the low thermodynamic stability of

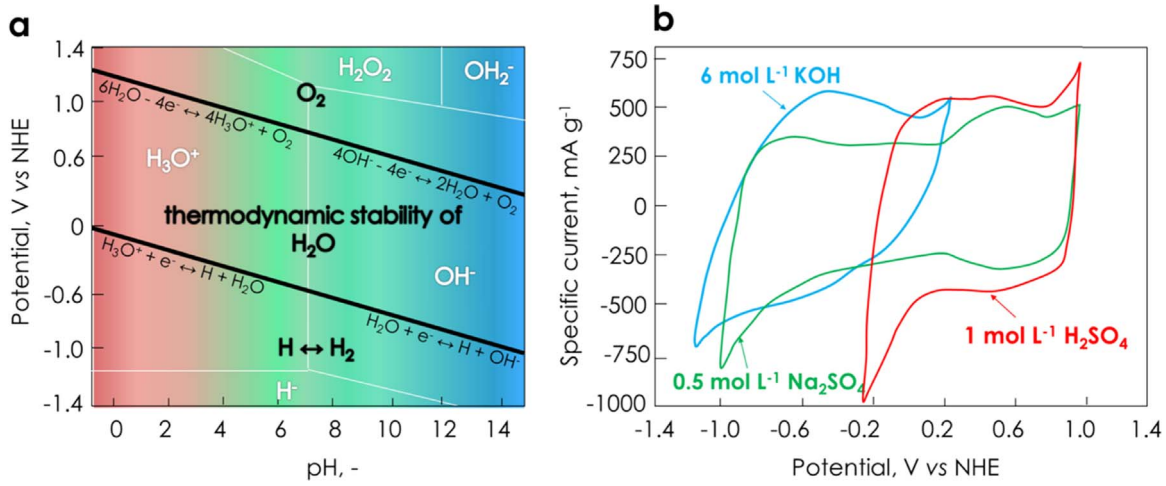

Fig. 10. (a) Potential-pH diagram indicating the thermodynamic limits of water marked by the two diagonal lines (based on [163]); (b) three-electrode cyclic voltammograms (2 mV s^{-1}) of activated carbon electrode in 6 mol L^{-1} KOH, 1 mol L^{-1} H_2SO_4 and 0.5 mol L^{-1} Na_2SO_4 [161].

water (Fig. 10a) is a major disadvantage of aqueous electrolytes. In theory, the reachable potential window of aqueous solutions is 1.23 V [157]. Practically, when porous carbon electrodes are used in ECs with the electrolytes traditionally implemented in aqueous electrochemical energy storage systems, e.g., H_2SO_4 and KOH, the usable potential window is generally less than 1 V [158–161]. By contrast, roughly twice larger potential window has been lately demonstrated when using neutral aqueous electrolytes, as shown by the three-electrode cyclic voltammograms of AC in 0.5 mol L^{-1} Na_2SO_4 (Fig. 10b) [158–161]. In the later medium, voltage values as high as 1.6 V were then found for AC/AC ECs [81,161] and even 2 V when using 1 mol L^{-1} Li_2SO_4 [162].

Such enhancement of the operating potential window has been attributed to the high over-potential for di-hydrogen evolution at the negative electrode, when compared to the thermodynamic limit of water reduction (lower diagonal in Fig. 10a) [164]. Indeed, under negative polarization, electrons are supplied to carbon and lead to the formation of nascent hydrogen and hydroxyl anions, according to Eq. (9) [165]:

$$H_2O + e^- \rightarrow H + OH^- \quad (9)$$

With highly porous electrodes, the trapped OH^- species are unable to leave the pores rapidly via diffusion or electro-migration, causing higher pH in intraparticle pores of the negative electrode than on its outer surface. Hence, according to the Nernst equation for the reduction equilibrium of water (10) [166]:

$$E_{H_2} = -0.059pH \quad (10)$$

the pH increase in the porosity causes a shift of the thermodynamic potential to lower values [164]. Such *in-situ* pH variations were confirmed on the surface of a carbon electrode when cathodic charging at −500 mA g^{-1} is applied, using 0.5 mol L^{-1} Na_2SO_4 electrolytic solutions of various initial pH by adding small amounts of 1 mol L^{-1} H_2SO_4 or 1 mol L^{-1}NaOH (Fig. 11) [167]. After 12 h of continuous cathodic charging, the pH reaches a value of ~ 11 for all the electrolytic solutions, except for the one with starting pH = 2, for which the value remains unchanged. The pH increase in the medium with initial pH = 4 is associated with either the formation of OH^- or reduced amount of H_3O^+, according to formula (11) [165]:

$$H_3O^+ + e^- \rightarrow H + H_2O \quad (11)$$

Considering the electrolytic solution with pH = 2, the reduction according to Eq. (11) results in a negligible pH increase, due to the excessive amount of hydronium ions adsorbed on the carbon surface.

Fig. 12 shows the three-electrode cyclic voltammograms of an activated carbon electrode in 1 mol L^{-1} Li_2SO_4, where each scan is

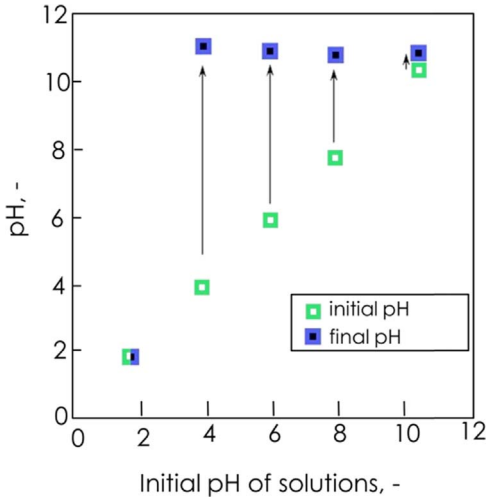

Fig. 11. Variation of pH values on the surface of an AC electrode after cathodic (−500 mA g^{-1}) charging for 12 h in solutions of various initial pH [167].

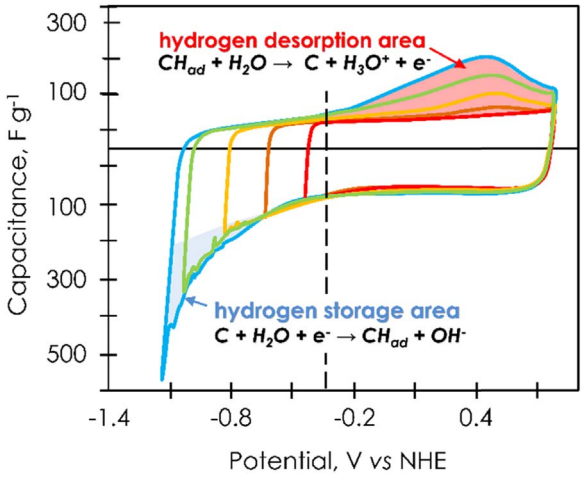

Fig. 12. Cyclic voltammograms (2 mV s^{-1}) of an activated carbon electrode in 1 mol L^{-1} Li_2SO_4 obtained by stepwise shift of the negative vertex potential. The dotted vertical line at −0.35 V vs NHE corresponds to the thermodynamic potential of water reduction (adapted from Ref. [175]).

obtained by shifting the negative vertex potential to lower value. At vertex potential higher than (or close to) the thermodynamic limit of water reduction, e.g., −0.35 V vs. NHE, only a capacitive current is recorded and the CVs have a rectangular shape characteristic of EDL charging. With decreasing of the negative vertex potential, a negative current leap appears, which is attributed to the formation of nascent hydrogen (Eq. (9)) and its chemisorption at the surface of pores (Eq. (12)) [168,169]

$$C + H \rightarrow CH_{ad} \quad (12)$$

Then, a peak related to hydrogen desorption appears during the anodic scan at around 0.4 V vs. NHE [164]. Owing to the aforementioned over-potential, the negative vertex potential beyond which gaseous di-hydrogen starts evolving on activated carbon electrode in 1 mol L^{-1} Li_2SO_4 is ca. −0.6 V vs. NHE (as observed by the oscillations due to bubbling on the CVs in Fig. 12). Hence, the high reversibility of the hydrogen chemisorption process provides an interesting option of Faradaic contribution in addition to the EDL capacitance. Activated carbons can store reversibly up to 2 wt% of hydrogen formed by electrochemical reduction of water under ambient pressure and temperature conditions [170–174].

Interestingly, hydrogen chemisorption was also evidenced for porous carbon electrodes in presence of a protic ionic-liquid (PIL), e.g., $[(C_2H_5)_3N^+H][TFSI^-]$ [176]. When the potential of a carbon electrode in PIL with low water content (< 20 ppm) is decreased, the $[(C_2H_5)_3N^+H]$ cation is reduced, and the produced nascent hydrogen is chemisorbed in the porosity of AC. In the presence of a higher amount of water (150 to 1000 ppm), the hydrogen storage mechanism involves hydronium cations (formed by the reaction of H_2O with $[(C_2H_5)_3N^+H]$) which serve as nascent hydrogen source (see Eq. (11)). The hydrogen recombination leading to H_2 evolution (the so-called Tafel reaction) is more favored if water is present in the electrolyte than with the dry PIL (< 20 ppm H_2O) [176], similarly to what is observed for aqueous electrolytes, where the protons from 3 mol L^{-1} H_2SO_4 are more available for the redox process at the electrode/electrolyte interface than in 6 mol L^{-1} KOH [165].

4.4. Redox-activity of electrolytic species at the positive electrode

As already described in Section 4.1, EDLCs store energy through reversible trapping of the charge carriers at the electrode/electrolyte interface without surface-confined redox reactions. However, if the electrolyte species reveal a redox activity, a symmetric AC/AC electrochemical capacitor may be transformed into a hybrid one. For example,

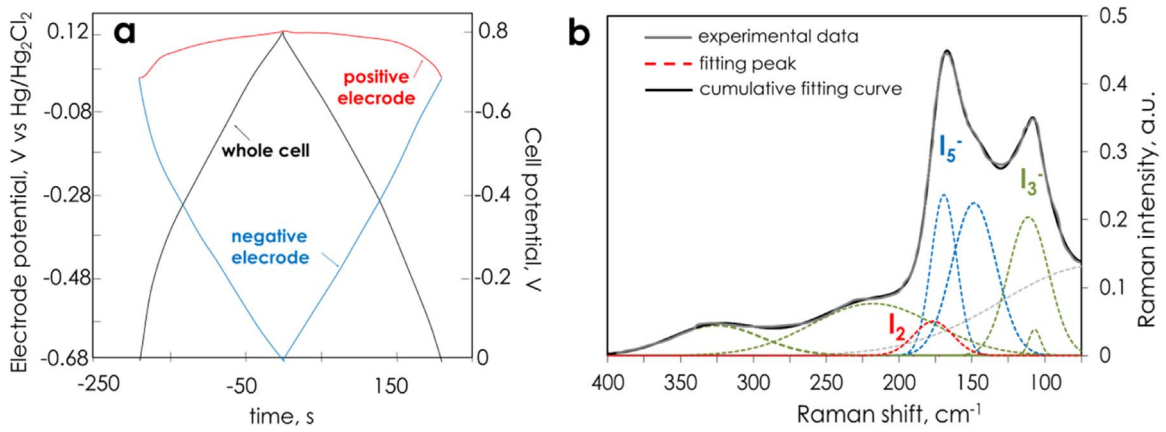

Fig. 13. (a) Galvanostatic charge/discharge (500 mA g^{-1}) of a two-electrode AC/AC cell in 1 mol L^{-1} KI solution (the cell was equipped with a SCE reference electrode to record the evolution of positive and negative electrode potentials when the system is charged/discharged) [179]. (b) *In-situ* Raman spectra recorded after potentiostatic polarization (750 mV vs SCE for 1 h) of an AC electrode in 2 mol L^{-1} NaI after subtracting the data recorded at OCV (adapted from Ref. [183]).

when potassium iodide is used as electrolyte in an AC/AC cell, reversible redox reactions (Eqs. (13)–(17)) [177,178] appear between 0 and 0.14 V vs Hg/Hg_2Cl_2 at the carbon/aqueous electrolyte interface of the positive electrode; at the same time, the negative electrode reveals an EDL behavior with the typical triangular shape of the GCPL curve (Fig. 13a) [179].

$$2I^- \leftrightarrow I_2 + 2e^- \quad (13)$$

$$3I^- \leftrightarrow I_3^- + 2e^- \quad (14)$$

$$2I_3^- \leftrightarrow 3I_2 + 2e^- \quad (15)$$

$$I_2 + I_3^- \leftrightarrow I_5^- \quad (16)$$

$$2I_2 + I^- \leftrightarrow I_5^- \quad (17)$$

Owing to the series dependence of the equivalent electrochemical circuit (Eq. (5)), when the capacity C_+ is much greater than the capacitance C_-, the overall capacitance of the system is essentially controlled by the capacitance of the EDL negative electrode ($C \approx C_-$), as opposed to the case of a typical EDLC where $C \approx 0.5C_-$. As a matter of fact, about two times larger capacitance of 240 F g^{-1} (calculated per average active mass of the two electrodes) is revealed for an AC/AC capacitor in 1 mol L^{-1} KI during galvanostatic cycling at 2 A g^{-1} as compared to 130 F g^{-1} for a cell with the same carbon electrodes (received by KOH activation) in 1 mol L^{-1} H_2SO_4 [179]. The maximum voltage reported for ECs in redox-active iodide electrolyte is around 1.2 V [180]; however, devices including Li_2SO_4 as supporting electrolyte together with KI can operate even up to 1.6 V, owing to the afore mentioned high over-potential of di-hydrogen evolution at the negative electrode (Section 4.3) [181]. Furthermore, owing to the redox activity of the $2I^-/I_2$ system, the self-discharge displayed by the cells using Li_2SO_4+KI is lower than in Li_2SO_4, which is another advantage of hybridization [150]. Recent works have demonstrated that the carbon/iodide interface is not established between the carbon surface and redox species dissolved in the electrolyte, but between polyiodides trapped inside the porosity of the positive electrode (which then operates as a traditional solid battery-type one) and the electrolyte. Since the redox species do not remain dissolved in the aqueous electrolyte, an insignificant charge redistribution is observed when the cell is set to open-circuit conditions [182].

In-situ Raman spectroscopy has been used to identify the species trapped in the porosity of AC under positive polarization and also to detect any structural modification of the electrode (i.e. changes in D and G peaks). The D and G bands and in particular the I_D/I_G ratio are not significantly changed after positive polarization of an AC electrode in NaI electrolyte [183]. Distinct Raman peaks characteristic of various polyiodide species appear at very similar Raman shifts as those disclosed for the AC ball-milled with the iodine solution [184]. For example, after one hour of potentiostatic polarization at 750 mV of an AC electrode in 2 mol L^{-1} NaI (Fig. 13b), a broad Raman peak at around 165 cm^{-1} related to I_5^- in presence of free I_2 (linear L-shaped and bent V-shaped units at around 148 and 169 cm^{-1}, respectively) was found [184]. A peak at 108 cm^{-1} discloses triiodide I_3^- units, whilst fit peaks at around 112, 218 and 328 cm^{-1} suggest additional formation of linear symmetric I_3^- chains (i.e., in the (benz)HI_3 structure).

Another proposed strategy to transform a positive AC electrode into a battery-type one (which operates in a narrow potential range), whereas the negative electrode remains of EDL-type, is to add hydroquinone (HQ) to 1 mol L^{-1} H_2SO_4 electrolyte [185,186]. However, when such cell is charged up to a voltage of 1 V, the high capacity induced by hydroquinone/p-benzoquinone (HQ/BQ) redox reaction at the surface of the positive electrode imposes a widening of the negative electrode potential range, and consequently a downshift of its minimum potential from −0.68 V to −0.96 V vs Hg/Hg_2SO_4. As a result, the electrolyte is decomposed and hydrogen is produced at the negative electrode (see Section 4.3), which entails a decrease of long-term stability of the cell in HQ/H_2SO_4 electrolyte, as demonstrated by a decrease of cell capacitance to 65% of its initial value after 4000 cycles up to 1 V [185]. Furthermore, BQ generated during charging dissolves in the electrolyte confined in the porosity of the positive electrode and diffuses towards the surface of the negative one. This so-called shuttle effect is considered to be the primary reason for the fast self-discharge of the system with HQ revealed by a voltage drop from 0.8 V to 0.05 V in 3100 s, as compared to a decrease to only 0.3 V after 11,500 s for the system without HQ [187]. For these reasons, it has been proposed to apply an ion-exchange membrane as separator to block the migration of the electrolytic species between the electrodes [187]. Another option to reduce self-discharge by supressing the shuttle effect, while gaining from enhanced capacitance values, is to choose a redox-active electrolyte converting into insoluble species during charging [187] or trapping the active species in the electrode porosity [179]. For instance, charging of an EC with 0.4 mol L^{-1} $CuSO_4$ in 1 mol L^{-1} H_2SO_4 results in the reduction of electroactive Cu^{2+} to Cu^0, which is insoluble in water and deposits onto the negative electrode [187]. Nevertheless, further cycling may lead to ion-starvation, while the porosity of carbon maybe simultaneously blocked, resulting in the reduction of negative electrode surface area.

In summary, combining porous carbon electrodes with appropriate electrolytes offers many possibilities for enhancing the performance of EDLCs, especially if getting high specific capacitance values is one of the main targets. Nevertheless, it should be always remembered that, due to the porous texture, the local environment (e.g., pH, electrolyte concentration) can be different in the porosity of the carbon electrode,

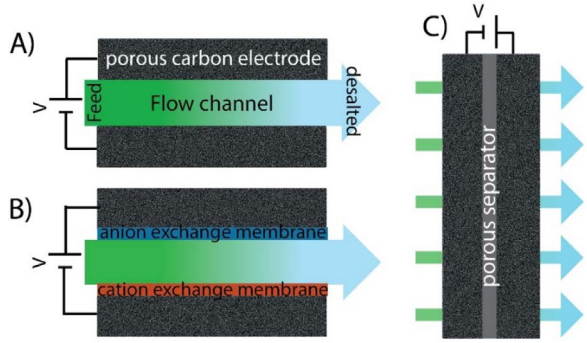

Fig. 14. Scheme of the main classes of static (film) electrode CDI systems, which include (A) CDI cells with feed flow between electrodes, (B) membrane CDI, and C) flow-through electrode CDI. Membranes can enable improved charge and energy efficiency of the desalination process [195], whereas flowing through the electrodes' macropores enables fast charging and application of compact cells [196].

on its outer surface, and in the bulk electrolyte. The electrode architecture may also favor the trapping of some inactive species (such as electrolyte decomposition products) [188,189], which reduce the electrode surface area available for the charge carriers, reducing the cycle-life of the cells.

5. Capacitive deionization (CDI)

5.1. Introduction

Capacitive deionization (CDI) is an emerging technology used to remove dissolved ions from a feed-water by storing them in a charged EDL within carbon micropores [18–20]. The main applications for CDI include energy efficient brackish water desalination and water softening. First conceptualized in the 1960s [190], a CDI cell consists of two microporous carbon electrodes sandwiching a porous dielectric separator, and the latter component also serves as the feed flow channel (Fig. 14A). The active electrode material used is most typically microporous activated carbon, and the electrode film consists of activated carbon particles, binder, and a conductive additive such as carbon black [191]. The electrode can also be a carbon aerogel monolith, or contain as active material carbon nanotubes, graphene, heteroatom doped carbons, and various metal oxide composite materials [19,124,192]. Applying a low voltage of around 1 V per electrode pair results in salt ions being electrosorbed into the micropores of the oppositely charged electrode, and desalination of the flowing feed-stream. Once the electrode pair is fully charged, discharging results in salt release into the feedwater, entailing an effluent brine stream. A variation of this basic cell architecture includes adding an ion exchange membrane in front of each electrode, which is termed membrane CDI (Fig. 14B). Including membranes enables improvement in desalination energy efficiency and ion removal capacity by blocking the parasitic co-ions current at the electrode/separator interface [193,194]. A second variation is to flow the feed directly through macropores in the porous electrodes instead of between the electrodes (an architecture known as flow-through electrode CDI, FTE CDI; Fig. 14C).

The most widely cited metric characterizing the performance of a CDI cell is the electrode salt adsorption capacity (SAC) [19], in units of mg g^{-1} (mg NaCl removed per g of electrode material). For calculating SAC, the salt adsorption is normalized by the mass of the electrode pair, which is typically the total electrode mass (not just the mass of the active microporous carbon material) [19]. For a charge half-cycle which proceeds to equilibrium, a SAC of up to ca. 15–20 mg g^{-1} can be obtained by microporous carbons [100,197]. Care must be taken in the control and reporting of the experimental conditions used for SAC measurements, as SAC can strongly depend on the initial salt concentration and applied voltage [198,199]. In terms of the design of porous carbon electrodes, one critical factor is the specific micropore volume (in mL g^{-1}), as increasing micropore volume enables a higher SAC during a complete charge half-cycle [200]. A predictive model applying increasing ion concentration with decreasing pore size has successfully described the SAC over a wide range of porous carbon materials with known pore size distributions [100]. The kinetics of the desalination process, quantified by a metric known as the average salt adsorption rate (ASAR), is not a function of the microporous carbon material alone, with important influence of the separator material, contact resistance, electrode thickness and electrode density [100,201].

Today, the most common application for CDI is brackish water desalination; however, CDI has also been investigated towards wastewater remediation, water softening, microfluidic sample preparation, and separations in organic solvents [19]. It is important to note that CDI is not limited to the common case of sodium chloride solutions and the removal of many other ions has been studied and demonstrated, such as potassium, boron, calcium, fluoride, or nitrate [202–204]. CDI with porous carbon electrodes is not typically utilized to desalt high salinity streams such as seawater, as the high initial co-ion concentration in micropores for such feeds leads to increased parasitic co-ion current and to low energy efficiency during cell charging [205,206]. The recent advent of CDI cells leveraging intercalation materials rather than porous carbons may allow for overcoming the latter limitations, by varying the mechanism of salt storage during cell charging from electrosorption in micropores to intercalation within bulk electrode materials [207,208]. Such cells have demonstrated values of SAC beyond what is attainable with porous carbons alone [209]. Other recent advances in electrode materials have leveraged surface functionalization of porous carbon electrodes to add charged surface groups into the micropores. This functionalization can change the dominant micropore electric charge compensation mechanism, and enable novel operational regimes such as inverted CDI, enhanced CDI, and extended-voltage CDI [199,210,211]. Surface functionalizing CDI electrodes has been shown to enable extended cell cycle life [212], or to improve electrode SAC [210].

5.2. EDLC and CDI: similarities and differences

At a first glance, CDI cells and EDLCs possess many similarities. Both concepts employ a pair of porous electrodes which store ions in the EDL within micropores during charging, and both must be operated in a two-stage process involving charge/discharge cycles. Further, for both cells, the most widely used electrode material for electrosorption is a porous carbon with significant microporosity. The similarities are emphasized by a CDI Ragone plot (called Kim-Yoon plot), shown in Fig. 15, whereby the salt adsorption capacity (SAC) vs. average salt adsorption rate (ASAR) for desalination by CDI cells is plotted [19,213]. This plot shows the tradeoffs in CDI cells between capacity and rate, and thus is similar in concept to the energy density vs. power density Ragone plot for energy storage often used to compare energy storage technologies such as electrochemical capacitors and batteries [214]. As is shown in Fig. 15, for constant voltage operation of a CDI cell, shorter cycles allow for higher salt adsorption rates at the expense of salt adsorption capacity.

Although many similarities exist, there are also many important differences between static electrode CDI cells and EDLCs. The most apparent is that, while EDLCs are operated without flowing the electrolytes, in CDI cells flow is required to deliver feedwater and extract desalted water from the cell. Another difference is in the choice of electrolyte, as EDLC cells often utilize relatively highly concentrated organic electrolytes (order 1 mol L^{-1}) or ionic liquids, yet CDI cells are limited to the feed-stream requiring treatment as the electrolyte, which is mainly aqueous and characterized by lower ion concentration (< 0.1 mol L^{-1}). Bridging this gap between CDI and EDLCs, an emerging application for CDI towards ion separations within organic solvent streams has only begun to be explored, yielding promising initial

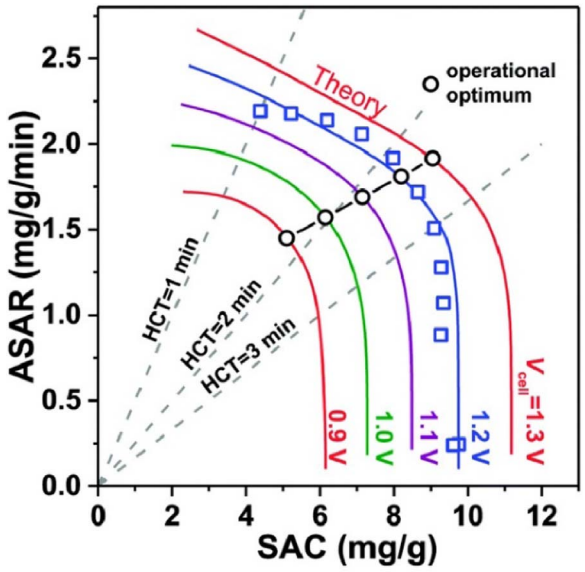

Fig. 15. A Kim-Yoon plot (a CDI Ragone plot) [213], based on Ref. [19], which presents the salt adsorption capacity (SAC) versus the salt removal rate (ASAR); V_{cell} is the cell voltage applied during the charging half-cycle, and HCT is the half cycle time of the CDI cell; shorter cycles can result in faster salt removal, yet lower amount of salt removed.

results such as higher SAC than can be achieved with aqueous solutions [215,216]. Another key difference related to choice of electrolyte is in the dynamics of the charging process in CDI and EDLCs. EDLCs are designed to avoid ion starvation (a local low concentration of ions) during cell charging [217], which is accomplished by the use of high ionic strength electrolytes. CDI systems, however, are designed for strong ion starvation as a means of desalination. Thus, the charging dynamics for EDLCs can be approximated by a suitable linear circuit model, such as a transmission line model with an RC-type charging time governing the dynamics [218]. By contrast, in CDI the dynamics can be highly nonlinear and are often characterized by multiple time scales [32].

The nature of electric charge compensation occurring in micropores is of importance in both EDLCs and CDI, but for different reasons [195]. In CDI, if charge compensation is dominated by the adsorption of counterions, then the feedstream (outside the micropores) is desalinated. However, if charge compensation were to occur exclusively due to ion swapping or dominated by co-ion expulsion, this would result in, no desalination of the feedstream, or an upconcentration of the feedstream, respectively (Fig. 16). To illustrate the crucial role of ion compensation mechanisms on CDI, recent experiments [212] and theory [199] have shown that adding charged surface groups, such as carboxyl or amine groups, to carbon micropores can cause a switch from counter-ion adsorption to co-ion expulsion as the dominant ion compensation mechanism, resulting in inverted cell operation (inverted-CDI). In this operational regime, the response of the CDI cell to applied voltages is completely inverted, as the feed is desalted on cell discharge and brine forms on cell charge. Quantifying the charge compensation mechanism is the CDI metric of charge efficiency, defined as the fraction of salt moles removed from the feed-water during cell charging to the moles of electric charge stored in the porous electrodes [198,205]. The latter ratio is always less than one due to the parasitic effect of co-ion current driving expulsion from the micropores, although charge efficiency may approach unity at high cell voltages [219]. For EDLCs, determining the charge compensation mechanism gives important insights into the complex interplay between pore size, ion size and ion solvation state with pore charge (for more details about charging mechanisms in EDLCs see Section 4.1) [142,145,206,220,221].

5.3. Flow-electrode CDI

Another major, emerging, category of CDI cell architecture uses flowing suspension electrodes rather than static film electrodes, an architecture termed flow electrode capacitive deionization (FCDI; Fig. 17). Static electrodes [222–224] are those made of an interconnected solid material, such as an activated carbon film, whereas flow electrodes consist of conductive carbon particles suspended in the flowing electrolyte (Fig. 17) [225,226]. First demonstrated by Jeon et al., [225,226] CDI utilizing flowable suspension electrodes has quickly become a highly active area of research due to the unique ability of these electrodes to enable continuous water desalination [227–229]. Rather than discharging the CDI cell itself, the carbon particles can flow out of the cell and be discharged downstream, for example in a mixing vessel [230], a second cell [231], or next compartment [227]. By contrast, CDI cells with static electrodes can only output desalted effluent for a certain time (the charge half-cycle), and then output brine (the discharge half-cycle). While enabling new functionalities, desalination by flowable electrodes also possesses drawbacks. Notably, static electrodes allow for typically orders of magnitude higher electrode electronic conductivity than flowable electrodes [232], and the latter often suffer from high flow viscosity increasing pump requirements over static systems [231,233]. Suspension electrodes have also been applied to EDLCs and flow battery systems for energy storage [234,235]; however, CDI is seen as an especially promising application for such electrodes. In EDLCs, flowable electrodes cause significant decrease in power density over that achieved by static electrode systems and also suffer from an enhanced self-discharge rate [236]. Such limitations are not crucial for CDI suspension electrodes, as they are typically discharged immedi-

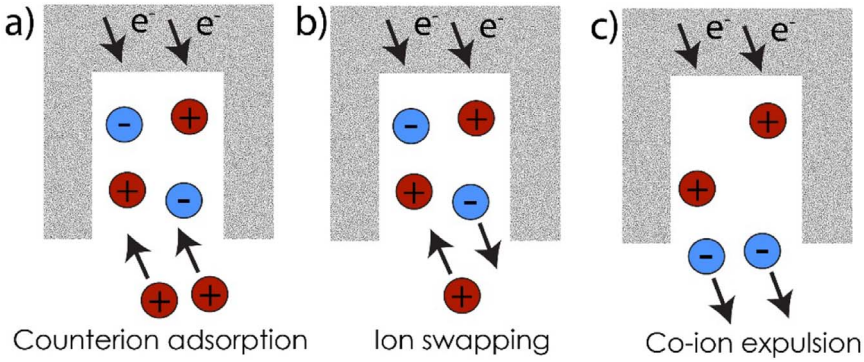

Fig. 16. Scheme of possible charge compensation mechanisms in carbon micropores. In all cases, two electrons are added to the carbon micropore surface (via an external power supply), which can result in several responses of the mobile ions: (a) counter-ion adsorption into the pore from the feedstream (the solution outside the micropore), (b) ion swapping between the pore and the bulk electrolyte, and (c) co ion expulsion to the bulk electrolyte. Only scenario a) results in the desalination of the bulk electrolyte, while all three scenarios store the same amount of electric charge (based on Ref. [199]).

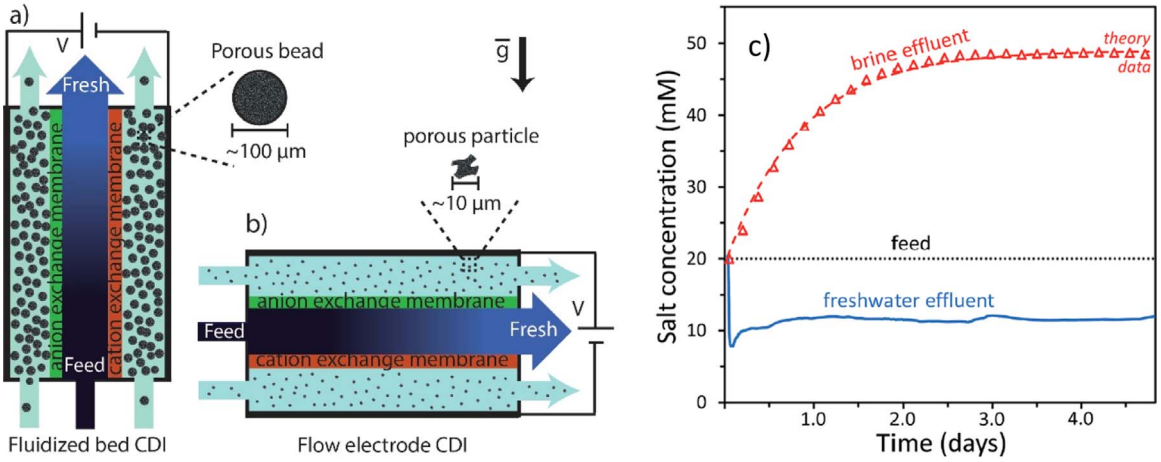

Fig. 17. (a, b) Comparison of flowable electrode CDI cells with (a) fluidized bed electrodes, and (b) flow electrodes (also known as slurry electrodes). While solid particles in slurries are entrained by the electrolyte, fluidized beds utilize larger particles and flow against gravity to enable formation of densely packed electrode structures. (c) Example data showing continuous and closed-loop desalination of a feed stream via fluidized bed capacitive deionization over a time period of several days [230].

ately after charging and do not have the primary function of storing energy [229].

Efforts in flow electrode materials research have so far been focused in empirically determining key electrode properties such as viscosity and electrical conductivity, and exploring different electrode configurations such as slurry, fluidized beds and combined suspension electrodes [228,237,238]. In an effort to improve electric charge transport through the flowable electrode, one key research thrust is the maximization of electrode carbon weight percent (wt%) (defined as the weight of flowing carbon divided by total flow electrode weight including carbon and electrolyte) [239]. Flow electrodes are typically slurries and are limited to ~ 20 wt% of carbon in order to remain flowable [98,228], but recently over 30 wt% carbon content was attained with fluidized bed electrodes, while flowing and desalting [230]. In fluidized beds, unlike slurries, carbon particles are subjected to significant gravitational force which allows for densely packed flowing electrode structures (Fig. 17). Towards optimal design of the porous carbon particles, the emphasis in FCDI shifts from high salt storage capability (high maximum SAC) to fast salt uptake by the flowing carbon particles (high ASAR). The design of carbon particles for fast salt uptake is coupled to the issue of improving electric charge transport through the electrode, and remains largely unexplored. For FCDI, it is more convenient to use a different set of metrics to describe the electrode performance than in static electrode CDI. One critical metric is current efficiency, defined as the flux of salt removed from the feed-water divided by Faraday's constant times the cell current, which is analogous to charge efficiency for static electrodes [19].

6. Capacitive energy harvesting from concentration gradients

The spontaneous mixing of solutions with differing concentrations, such as sea and river water, thermolytic salts, or solutions with varying gas phase CO_2 concentration results in a release of energy. In particular, the mixing of river and sea water results in the release of an estimated 2.6 TW per year worldwide [240]. Mixing energy harvesting refers to a set of technologies which can capture part of this energy by converting it to electricity [16,17]. Classic mixing energy harvesting technologies include pressure retarded osmosis (PRO) [241] and reverse electrodialysis (RED) [242,243], and when applied to sea and potable water, these can be described as the inverse process of water desalination via reverse osmosis and electrodialysis, respectively. In 2009, Brogioli introduced a novel mixing energy harvesting technology leveraging a set of charged capacitive porous carbon electrodes, termed capacitive double-layer expansion (CDLE) [244–246]. Recent CDLE cells utilize an architecture similar to that of typical CDI and EDLC cells, consisting of two porous carbon electrodes and a separator [247]. A typical operation cycle begins with charging the cell while it contains a relatively concentrated electrolyte, and then while holding the cell electric charge constant, to replace the electrolyte by one more dilute [31]. This results in a decrease of the cell capacitance as the EDLs in the porous electrodes expand, since ions re-arrange to be further from the charged carbon surfaces due to the effect of diffusion (see Eq. (2)). As cell charge is held constant, the net effect is that in the dilute electrolyte, the CDLE cell voltage increases [248]. Thus, subsequent discharging of the cell can release more energy than was used to charge the cell in concentrated electrolyte, due to the higher cell potential at discharge (in the dilute electrolyte). For CDLE, one important criterion is to maintain a low leakage current while the cell is charged, as without careful attention to this parameter, the power required to maintain the cell's potential can become larger than the power outputted during device operation [245]. In 2012, Brogioli et al. [245] demonstrated that a charged CDLE cell, with symmetric porous carbon electrodes held at constant charge, exhibited a drift in voltage due to self-discharge (leakage current) which continued until each electrode reached its spontaneous potential (potential of the electrodes relative to a reference electrode when 0 V is applied to the CDLE cell) relative to a suitable reference electrode. By judiciously choosing materials and cell voltage to minimize leakage current, the authors demonstrated a CDLE cell delivering a maximum power density of 50 mW cm^{-2} (Fig. 18) [245]. Recently, research has focused on surface functionalization of the porous carbons to add charged surface groups, such as carboxyl groups (similar to modifications used for CDI electrodes, see Section 5), or to enable electrode proton selectivity [249,250].

The past several years have seen the rapid development of several technologies for harvesting mixing energy related to CDLE including the capacitive Donnan potential (CDP) method, the utilization of bioelectrochemical cells to drive the harvesting process, and also the use of flow (or slurry) electrodes [17,251,252]. These techniques, as well as the original CDLE method, fall all under the umbrella term “capacitive mixing” or, for short, “CAPMIX”.CDP is an alternative method for mixing energy harvesting using porous carbon electrodes together with ion exchange membranes [17]. One anion and one cation exchange membranes are placed on the separator side of the porous carbon electrodes, and the variations between the membrane Donnan potentials can drive the charging and discharging of the porous electrodes without the need for an external power supply. When a dilute solution replaces the more concentrated one, the cell potential rises, and then decreases when the more concentrated solution is entered into the system, and this charging and discharging results in a

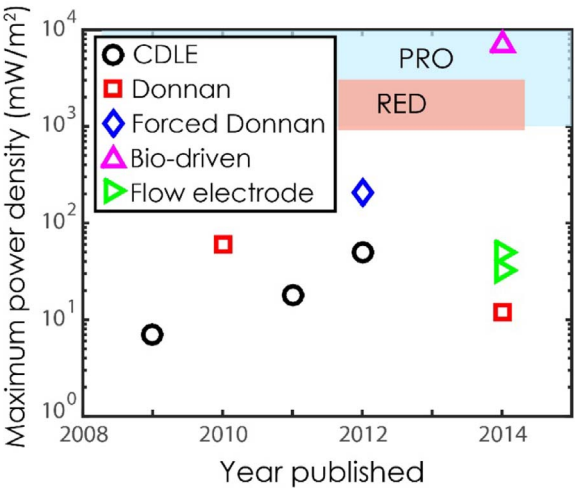

Fig. 18. A historical review of the maximum power density achieved by various capacitive mixing technologies, compared to the power densities achieved by traditional mixing energy harvesting, pressure retarded osmosis (PRO, blue region) and reverse electro dialysis (RED, red region). Legend: CDLE = capacitive double-layer expansion.

current response of the cell when connected to a load. Recently, it has been demonstrated that ion exchange membranes can be replaced by a polyelectrolyte coating carbon electrodes to exploit the Donnan potential [253]. While CDP can be used without requiring an external power source, an increase in the cell power output can be achieved if charge from an external power supply is added to the cell during the charging step. The latter is known as forced CDP, and has demonstrated maximum power density higher than 200 mW m^{-2}. Forced CDP devices have been built which operate within the electric field set by a bioelectrochemical fuel cell system with a microbial fuel cell anode and oxygen cathode [252]. Such a device showed a remarkable maximum power density of 7 W m^{-2}, on par with the power obtainable from state-of-the-art PRO system (Fig. 18) [252].

Recently, the advent of carbon slurry electrodes for water desalination in CDI systems has also translated to energy harvesting by CAPMIX systems [228]. Like in CDI, flow electrodes enable functionalities in mixing energy harvesting over what can be obtained from static electrode systems. The main benefit is the demonstrated ability for a constant and continuous power output from the harvesting system, unlike static electrode CDLE systems which deliver their maximum power at the beginning of the discharge stages, but then deliver less power as the discharge progresses. This benefit was first shown by Porada et al., who used a single cell with slurry electrodes and ion exchange membranes to demonstrate continuous power generation of 32 mW m^{-2} [228]. Hatzell et al. demonstrated a flow electrode CAPMIX system which delivered continuously 50 mW m^{-2}, when configured as a four reactor system in series [251].

As CAPMIX is a very new, yet fast emerging technology, there remain many questions towards its long term viability. One key question which needs to be answered is about the costs and energy requirements associated with solution pre-treatment and fouling for these CAPMIX technologies. Such requirements are significant, and were shown to be serious constraints towards commercialization of PRO systems for the mixing of river and sea water [254]. In the CAPMIX technological family, there are a wide variety of cell architectures used and so there may also be wide differences in pre-treatment requirements and fouling characteristics. For example, the technologies range from the use of relatively robust porous carbon electrodes in CDLE cells, all the way to highly complex bioelectrochemical cells with ion exchange membranes. Compared to the more mature technologies of PRO and RED, highly optimized performance from CAPMIX systems has not yet been attained. In Fig. 18, a historical review of the development of the CAPMIX field is presented through comparison of maximum attained power densities. The comparison of powers obtained to that seen in the more mature mixing energy harvesting technologies of PRO and RED highlights that CAPMIX is generally at lower power density. The bioelectrochemical system of Hatzell et al. has shown the most promising power delivery to date, attaining PRO levels [252].

7. Capacitive actuation

As described in Section 4.2, the adsorption of ions into the pores of carbon upon polarization can entail dimensional changes in the electrodes of an EDLC [149] and affect its performance during cycling due to conductivity decrease of the electrode material. However, the change in electrodes volume can also be a desired effect, for example in case of ionic electroactive polymer (iEAP) composites, also known as ionic capacitive laminates (ICLs). When charging an ICL, one of the electrodes contracts while the other expands [255], and as a result the material acts as an actuator and converts electrical energy into mechanical and *vice versa* [256,257]. In opposition to classical EDLC or CDI cells, where the electrodes are in physical contact with the separator, the carbon electrodes of ionic capacitive laminates are bonded together with the separating membrane, and the whole laminate is filled with the electrolyte as shown in Fig. 19a. Such three-layer design exploits small volume changes in the electrodes and translates them into a maximum mechanical response needed for the realization of bending devices [258–260].

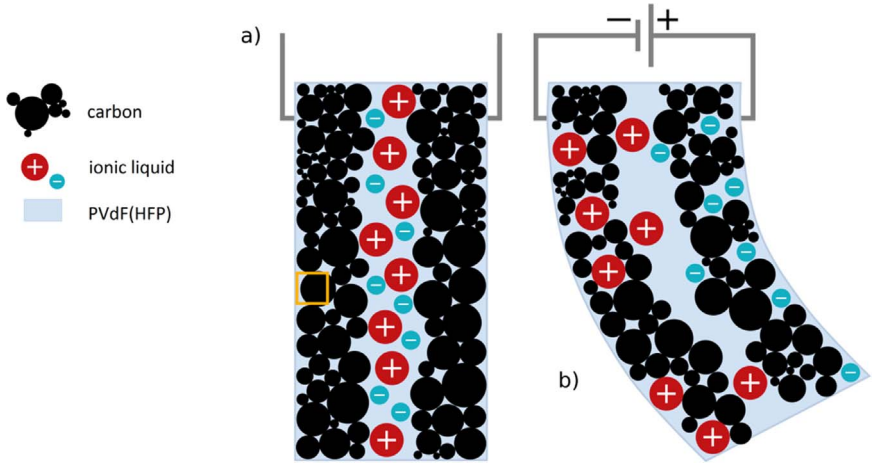

Fig. 19. (a) Three-layer actuator design with electrodes bonded together with the separating membrane and filled with the electrolyte. (b) Actuator after a voltage stimulus is applied [267].

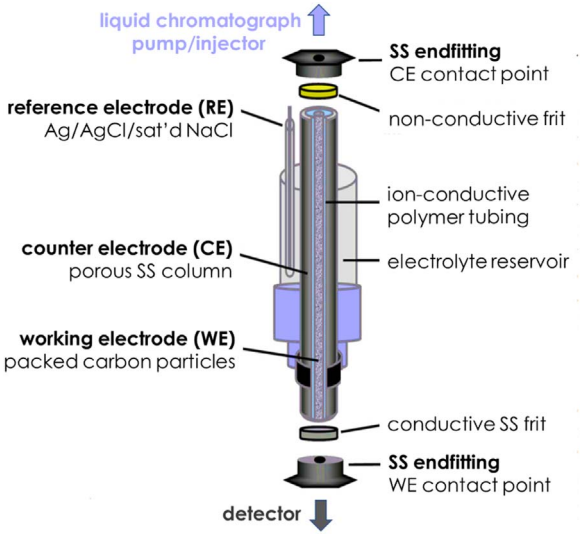

Fig. 20. Schematic illustration of an electrochemically modulated liquid chromatography column [241].

The mechanical operation of an iEAP actuator is explained by ions movement triggered by charging and discharging, yet the exact mechanism causing the strain difference in the material is still an open debate for several existing theories. In 1999, Baughman et al. constructed the first carbon-based iEAP actuator using CNT bucky paper electrodes stick with a silicone adhesive to both sides of a polyamide tape separator [261]. The volume change was attributed to quantum chemical charge injection, which directly changes the C-C bond length. Later, electrodes containing a mixture of carbon nanotubes, ionic liquid and polymer binder were proposed to build a bucky-gel actuator with improved bending magnitude [258]. Owing to the smaller concentration of CNTs in this type of actuator (as compared to Ref. [261]), the authors argued that the intercalation of ions between the concentric carbon layers of multi-walled carbon nanotubes and the resulting volumetric change should be considered as the primary mechanism in the strain generation of iEAP actuators. The size of ions plays an important role during the electrically induced intercalation mechanism: the larger ions (usually cations) generate an expansion of one of the electrodes (usually the negatively charged electrode), and smaller ions (usually anions) allow the contraction of the second electrode (usually the positive one) (Fig. 19b) [262]. It has been also suggested that different mobility between cations and anions could explain the actuation mechanism [263].

So far, various carbon materials, such as carbon nanotubes [261,264], graphene [265], carbide-derived carbons [266,267], carbon aerogels [268], and activated carbons [266] have been implemented in ICLs. Actuators made of these materials display high mechanical flexibility, structural simplicity, absence of acoustic noise during actuation and high strength-to-mass ratio. In addition, the actuators utilizing carbon electrodes can be designed with suitable size and shape, and may be used in various environments (ambient conditions, under vacuum and in liquids).

A new type of quasi-all-solid actuator has been obtained by using a gel ionic liquid electrolyte together with a soft actuator material produced through a layer-by-layer casting method [258]. In this technique, films are obtained by pouring a gel electrode suspension composed of carbon particles well-dispersed in a solvent on a gelatinous membrane; then, the membrane is sandwiched between the two electrodes by hot-pressing.

The layer-by-layer casting method has been also used to assemble actuators with TiC-derived carbons (CDCs) synthesized by chlorination at 400 °C, 800 °C and 950 °C, and having S_{BET} of 1113 m^2 g^{-1}, 1470 m^2 g^{-1} and 1843 m^2 g^{-1}, and average pore size of 0.65 nm, 0.97 nm and 1.02 nm, respectively [234]. Bending strain values of 0.09% to 0.62% have been found for CDC-400 °C and CDC-950 °C, respectively [234]. The actuator based on the Mo_2C-based carbon with the largest specific surface area and average pore size demonstrated the fastest response and contributed to the largest strain values.

A competitive technology for preparing carbon-based actuator laminates is called Direct Assembly Process (DAP) [259]. In this method, an electrode solution is sprayed onto the two sides of an electrolyte-soaked polymer membrane to form ICLs. By using DAP, it is easy to manufacture ICLs with different electrode thicknesses, just by spraying a different number of electrode layers. To improve the electronic conductivity, the electrodes may be covered with current collectors made of 100 nm thick gold foil. Various carbons (CDC, carbon aerogel and activated carbons) have been used in the DAP process for preparing actuator materials.

Recently, new methods have been introduced to manufacture thin actuator electrodes at a large scale. For example, spin coating or layer-by-layer deposition of the electroactive material around a woven fabric substrate allows actuators with good repeatability to be obtained [269]. In general, ionic capacitive laminates can be used for several applications, e.g., for moving small objects, as mechano-electrical or humidity sensors, energy storage devices or energy harvesting from mechanical movement or humidity gradients [270].

8. Potential-controlled chromatography

Besides the aforementioned technologies, the electrosorption of charged species can be also employed for an enhanced type of liquid chromatography, called either potential-controlled chromatography [21], or electrochemically modulated liquid chromatography (EMLC) [271,272], or electrochemically modulated liquid chromatographic separation [273]. A typical column used for EMLC is based on a three-electrode configuration, where a conductive carbon material is used both as stationary phase and working electrode (WE), whereas a porous stainless steel cylinder acts as counter electrode (CE) (Fig. 20). An ion-conductive polymer film is situated between the carbon working electrode and the stainless steel cylinder counter electrode to prevent electrically short-circuiting the WE and CE. The column is fitted with a reservoir filled with an electrolyte, which surrounds the stainless steel (SS) cylinder; the reference electrode (RE) is placed inside this reservoir. When a potential difference is applied between WE and CE, the electrostatic interactions between the analyte and the conductive stationary phase are modified, and in consequence, the chromatographic retention is changed. Hence, the selectivity of the column can be dynamically manipulated by adjusting the potential which is applied between the stationary phase and the counter electrode. This feature enables also to enhance the concentration of certain molecules by introducing time-controlled withholding/releasing. The properties of the column can be adapted for various applications by changing/modifying the carbon material. So far, glassy carbon [272], carbon fibers [271], porous graphitic carbon [274] have been used as conductive stationary phase.

EMLC has been used for example for the extraction of seven triazines from soil samples by varying the potential of the stationary phase and the pH of the analyte [273]. In combination with different separation methods, such as reversed-phase capillary liquid chromatography, EMLC is also a powerful analysis technique.

9. Conclusion

Carbons characterized by highly extended surface area and pores which match with the size of electrolyte ions appear as the most suitable electrode materials for capacitive applications, where a high amount of charge should be efficiently accumulated in an EDL. The high interest in carbons is also on account of their high conductivity, versatility of morphologies, ability to tune the porous texture, controll-

ability of surface functionalities, high natural abundance of precursors and low cost. Nevertheless, for each of the applications detailed in this review, it is important to look through the specific set of desires in order to select the most appropriate carbonaceous material.

The parameters closely connected with the porous texture (specific surface area, pore volume, size and shape of pores, tortuosity) play an important role in the capacitive performance. One should be always aware that the EDL composition, and its formation mechanisms in the confined porosity of an electrode, is different from the models presented for an electrode flat surface. During charging, the EDL formed inside micropores is composed not only of single counter-ionic species, but of co-ions and solvent molecules. Moreover, the specific surface area of porous carbon electrodes estimated by use of a gas probe (the most often nitrogen) cannot be directly considered for predicting the capacitive performance in presence of electrolyte species of different size and affinity with pore walls.

When considering the capacitive technologies, the importance of electrode architecture, thickness and other physical parameters cannot be ignored. For example, if the ion transport rate should be improved to ensure the charge storage, materials with a large external surface area (such as graphene, carbon onions or carbon nanotubes) should be preferred to provide a hierarchic transport pathway. When considering energy efficient water desalination with flowable carbon suspension electrodes, the particle shape and agglomeration, and viscosity of suspension become important factors to maximize the ratio of moles of salt removed from the water feedstock to the moles of electrons transferred during cell charging.

As it is well-know, to some extent, a high surface area of carbon electrodes supports their capacitive properties; yet, it is not often considered that reversible trapping of inorganic charge carriers in the electrode pores is an opportunity for faradaic contributions as well as enhancement of operating voltage. In EDLCs with neutral aqueous electrolytes and highly porous electrodes, the trapped OH^- species cause a local pH change inside the pores of the negative electrode. A higher pH in the porosity of the electrode than on its outer surface entails the over-potential for di-hydrogen evolution, which enables the AC/AC capacitors in (Li, K, $Na)_2SO_4$ to reach roughly twice larger potential window than in the 'standard' water media (H_2SO_4, KOH). Furthermore, if species trapped in the porosity of a carbon electrode reveal a redox activity, a symmetric carbon/carbon EDLC can be transformed into a hybrid one. For instance, the utilization of hydroquinone (as an additive to H_2SO_4) or iodide (as electrolyte itself or added to neutral aqueous sulfate solutions) leads to transform the positive electrode into a battery-type one, owing to redox reactions which take place at the carbon/electrolyte interface, whereas the negative electrode remains of the EDL-type. Hence, such hybridization demonstrates potentialities for gaining in capacitance, and consequently energy of eco-friendly capacitive storage devices.

Undoubtedly, high surface area nanostructured carbons and electrodes manufactured from these carbons do reveal benefits and limitations in the various capacitive technologies considered in this paper. Therefore, in order to guide researchers and engineers in finding the most proper carbon for a certain technology, our aim was to review the sets of specific requirements expected from electrode materials. Hence, on this basis, most of the materials which have been suggested as alternative to high surface area nanostructured carbons for capacitive technologies are generally not realistic because of their higher cost and very often fair performance. As also highlighted in the manuscript, besides the huge role of the electrodes in these technologies, the influence of the electrolytic solution on the EDL formation in the porosity of carbon electrodes and on the resulting stability potential window cannot be neglected. In this context, the new opportunities offered by the recent claims on e.g., so-called water-in-salt electrolytes represent an interesting research direction which should be investigated to develop high energy eco-friendly electrochemical capacitors.

Acknowledgements

The Polish National Science Center (NCN) is acknowledged for supporting the OPUS project UMO 2014/15/B/ST4/04957. The Polish Ministry of Science and Higher Education is acknowledged for funding the 03/31/DSPB/0334/2017 and 03/31/DSMK/0348/2017 grants.

References

[1] J.K. Kaldellis, Stand-Alone and Hybrid Wind Energy Systems: Technology, Energy Storage and Applications, CRC Press, Boca Raton, 2010.
[2] L.L. Zhang, Z. Lei, J. Zhang, X. Tian, X.S. Zhao, Supercapacitors: electrode materials aspects, in: Encyclopedia of Inorganic and Bioinorganic Chemistry, John Wiley & Sons, Ltd, 2011.
[3] S. Zhang, N. Pan, Adv Energy Mater 5 (2015) (article 1401401).
[4] C. Vix-Guterl, E. Frackowiak, K. Jurewicz, M. Friebe, J. Parmentier, F. Béguin, Carbon 43 (2005) 1293–1302.
[5] Z. Kovac, C.J. Sambucetti, Importance of electrical double layer in technological applications, in: O.J. Murphy, S. Srinivasan, B.E. Conway (Eds.), Electrochemistry in Transition: From the 20th to the 21st Century, Springer, US, Boston, MA, 1992, pp. 39–49.
[6] F. Béguin, V. Presser, A. Balducci, E. Frackowiak, Adv. Mater. 26 (2014) 2219–2251.
[7] E. Frackowiak, Phys. Chem. Chem. Phys. 9 (2007) 1774–1785.
[8] E. Frackowiak, F. Béguin, Carbon 39 (2001) 937–950.
[9] G. Wang, L. Zhang, J. Zhang, Chem. Soc. Rev. 41 (2012) 797–828.
[10] A.G. Pandolfo, A.F. Hollenkamp, J Power Sources 157 (2006) 11–27.
[11] P. Simon, Y. Gogotsi, Nat. Mater. 7 (2008) 845–854.
[12] Y. Zhai, Y. Dou, D. Zhao, P.F. Fulvio, R.T. Mayes, S. Dai, Adv. Mater. 23 (2011) 4828–4850.
[13] L.L. Zhang, X.S. Zhao, Chem. Soc. Rev. 38 (2009) 2520–2531.
[14] B.E. Conway, Electrochemical Supercapacitors: Scientific Fundamentals and Technological Applications, Springer, US, 2013.
[15] F. Béguin, E. Frackowiak, Carbons for Electrochemical Energy Storage and Conversion Systems, CRC Press, Boca Raton, 2009.
[16] B.B. Sales, M. Saakes, J.W. Post, C.J.N. Buisman, P.M. Biesheuvel, H.V.M. Hamelers, Environ. Sci. Technol. 44 (2010) 5661–5665.
[17] M.F.M. Bijmans, O.S. Burheim, M. Bryjak, A. Delgado, P. Hack, F. Mantegazza, S. Tenisson, H.V.M. Hamelers, Energy Procedia 20 (2012) 108–115.
[18] L. Han, K.G. Karthikeyan, K.B. Gregory, J. Electrochem. Soc. 162 (2015) E282–E288.
[19] M.E. Suss, S. Porada, X. Sun, P.M. Biesheuvel, J. Yoon, V. Presser, Energy Environ. Sci. 8 (2015) 2296–2319.
[20] M. Noked, A. Soffer, D. Aurbach, J. Solid State Electrochem. 15 (2011) 1563–1578.
[21] F. Kocak, K. Vuorilehto, J. Schrader, D. Sell, J. Appl. Electrochem. 35 (2005) 1231–1237.
[22] I. Must, F. Kaasik, I. Põldsalu, L. Mihkels, U. Johanson, A. Punning, A. Aabloo, Adv. Eng. Mater. 17 (2015) 84–94.
[23] H. Von Helmholtz, Ann. Phys. Chem. 89 (1853) 211–233.
[24] H. Ji, X. Zhao, Z. Qiao, J. Jung, Y. Zhu, Y. Lu, L.L. Zhang, A.H. MacDonald, R.S. Ruoff, Nat. Commun. 5 (2014) (article 3317).
[25] P.K. Shen, C.Y. Wang, S.P. Jiang, X. Sun, J. Zhang, Electrochemical Energy: Advanced Materials and Technologies, CRC Press, Boca Raton, 2016.
[26] D.L. Chapman, Philos. Mag. 25 (1913) 475–481.
[27] O. Stern, Zeit . Elektrochem. 30 (1924) 508–516.
[28] D.C. Grahame, Chem. Rev. 41 (1947) 441–501.
[29] P.M. Biesheuvel, Y. Fu, M.Z. Bazant, Russ. J. Electrochem. 48 (2012) 580–592.
[30] M.S. Kilic, M.Z. Bazant, A. Ajdari, Phys. Rev. E 75 (2007) (article 021502).
[31] R.A. Rica, R. Ziano, D. Salerno, F. Mantegazza, D. Brogioli, Phys. Rev. Lett. 109 (2012) (article 156103).
[32] P.M. Biesheuvel, M.Z. Bazant, Phys. Rev. E 81 (2010) (article 031502).
[33] J.O.M. Bockris, M.A.V. Devanathan, K. Muller, Proc. R. Soc. Lond. A: Math. Phys. Eng. Sci., 274, 1963, pp. 55–79.
[34] G. Ballou, Handbook for Sound Engineers, Focal Press, Abingdon, 2015.
[35] Y. Gogotsi, V. Presser, Carbon Nanomaterials, 2nd ed., CRC Taylor & Francis, Boca Raton, 2014.
[36] T.E. Rufford, D. Hulicova-Jurcakova, Z. Zhu, G.Q. Lu, Electrochem. Commun. 10 (2008) 1594–1597.
[37] L. Wei, M. Sevilla, A.B. Fuertes, R. Mokaya, G. Yushin, Adv. Energy Mater. 1 (2011) 356–361.
[38] P. Kleszyk, P. Ratajczak, P. Skowron, J. Jagiello, Q. Abbas, E. Frąckowiak, F. Béguin, Carbon 81 (2015) 148–157.
[39] D. Wu, Z. Li, M. Zhong, T. Kowalewski, K. Matyjaszewski, Angew. Chem. Int. Ed. 53 (2014) 3957–3960.
[40] A.K. Geim, K.S. Novoselov, Nat. Mater. 6 (2007) 183–191.
[41] C. Liu, F. Li, L.-P. Ma, H.-M. Cheng, Adv. Mater. 22 (2010) E28–E62.
[42] W. Zhang, C. Xu, C. Ma, G. Li, Y. Wang, K. Zhang, F. Li, C. Liu, H.M. Cheng, Y. Du, N. Tang, W. Ren, Adv. Mater. 29 (2017) (article 1701677).
[43] V. Strauss, K. Marsh, M.D. Kowal, M. El-Kady, R.B. Kaner, Adv. Mater. 30 (2018) (article 1704449).
[44] Y. Shao, M.F. El-Kady, L.J. Wang, Q. Zhang, Y. Li, H. Wang, M.F. Mousavi, R.B. Kaner, Chem. Soc. Rev. 44 (2015) 3639–3665.

[45] D. Yanfeng, W. Zhong-Shuai, R. Wencai, C. Hui-Ming, B. Xinhe, Sci. Bull. 62 (2017) 724–740.
[46] S. Wang, Z.-S. Wu, S. Zheng, F. Zhou, C. Sun, H.-M. Cheng, X. Bao, ACS Nano 11 (2017) 4283–4291.
[47] D. Li, M.B. Müller, S. Gilje, R.B. Kaner, G.G. Wallace, Nat. Nanotechnol. 3 (2008) 101–105.
[48] S. Gan, L. Zhong, T. Wu, D. Han, J. Zhang, J. Ulstrup, Q. Chi, L. Niu, Adv. Mater. 24 (2012) 3958–3964.
[49] Y. Sun, Q. Wu, G. Shi, Energy Environ. Sci. 4 (2011) 1113–1132.
[50] Y. Xu, Z. Lin, X. Zhong, X. Huang, N.O. Weiss, Y. Huang, X. Duan, Nat. Commun. 5 (2014) (article 4554).
[51] C. Cheng, F. Yuqi, G. Jianhang, W. Liming, P. Stefano, M. Liqiang, J. Phys. D: Appl. Phys. 51 (2018) (article 113002).
[52] M. Cinke, J. Li, B. Chen, A. Cassell, L. Delzeit, J. Han, M. Meyyappan, Chem. Phys. Lett. 365 (2002) 69–74.
[53] C. Niu, E.K. Sichel, R. Hoch, D. Moy, H. Tennent, Appl. Phys. Lett. 70 (1997) 1480–1482.
[54] T. Chen, L. Dai, Mater. Today 16 (2013) 272–280.
[55] M. Pérez-Cabero, I. Rodríguez-Ramos, A. Guerrero-Ruíz, J. Catal. 215 (2003) 305–316.
[56] M.S. Dresselhaus, I.L. Thomas, Nature 414 (2001) 332–337.
[57] W. Lu, L. Qu, K. Henry, L. Dai, J. Power Sources 189 (2009) 1270–1277.
[58] C. Du, N. Pan, J. Power Sources 160 (2006) 1487–1494.
[59] D. Luxembourg, X. Py, A. Didion, R. Gadiou, C. Vix-Guterl, G. Flamant, Microporous Mesoporous Mater. 98 (2007) 123–131.
[60] T. Kim, S. Lim, K. Kwon, S.-H. Hong, W. Qiao, C.K. Rhee, S.-H. Yoon, I. Mochida, Langmuir 22 (2006) 9086–9088.
[61] E. Bae, N.D. Kim, B.K. Kwak, J. Park, J. Lee, Y. Kim, K. Choi, J. Yi, Carbon 48 (2010) 3676–3681.
[62] M.E. Plonska-Brzezinska, L. Echegoyen, J. Mater. Chem. A 1 (2013) 13703–13714.
[63] M. Zeiger, N. Jackel, V.N. Mochalin, V. Presser, J. Mater. Chem. A 4 (2016) 3172–3196.
[64] C. Portet, G. Yushin, Y. Gogotsi, Carbon 45 (2007) 2511–2518.
[65] J.K. McDonough, Y. Gogotsi, Electrochem. Soc. Interface 22 (2013) 61–66.
[66] E.G. Bushueva, P.S. Galkin, A.V. Okotrub, L.G. Bulusheva, N.N. Gavrilov, V.L. Kuznetsov, S.I. Moiseekov, Phys. Status Solidi (b) 245 (2008) 2296–2299.
[67] A. Balducci, C. Schütter, Bol. Grupo Esp. Carbón (2015) 2–5.
[68] J. García-Martínez, K. Li, M.E. Davis, Mesoporous Zeolites: Preparation, Characterization and Applications, Wiley, Weinheim, 2015.
[69] R. Scipioni, P.S. Jørgensen, D.-T. Ngo, S.B. Simonsen, Z. Liu, K.J. Yakal-Kremski, H. Wang, J. Hjelm, P. Norby, S.A. Barnett, S.H. Jensen, J. Power Sources 307 (2016) 259–269.
[70] R.E. Franklin, Proc. R. Soc. Lond. Ser. A Math. Phys. Sci.. 209, 1951, pp. 196–218.
[71] J.S. McDonald-Wharry, M. Manley-Harris, K.L. Pickering, Energy Fuels 30 (2016) 7811–7826.
[72] H.F. Stoeckli, F. Kraehenbuehl, Carbon 22 (1984) 297–299.
[73] R.B. Marichi, V. Sahu, R.K. Sharma, G. Singh, Efficient, sustainable, and clean energy storage in supercapacitors using biomass-derived carbon materials, in: L.M.T. Martínez, O.V. Kharissova, B.I. Kharisov (Eds.), Handbook of Ecomaterials, Springer International Publishing, Cham, 2017, pp. 1–26.
[74] Z. Li, L. Zhang, B.S. Amirkhiz, X. Tan, Z. Xu, H. Wang, B.C. Olsen, C.M.B. Holt, D. Mitlin, Adv. Energy Mater. 2 (2012) 431–437.
[75] D. Lozano-Castelló, M.A. Lillo-Ródenas, D. Cazorla-Amorós, A. Linares-Solano, Carbon 39 (2001) 741–749.
[76] Z. Hu, M.P. Srinivasan, Y. Ni, Carbon 39 (2001) 877–886.
[77] M. Molina-Sabio, F. Rodríguez-Reinoso, F. Caturla, M.J. Sellés, Carbon 33 (1995) 1105–1113.
[78] D. Lozano-Castelló, D. Cazorla-Amorós, A. Linares-Solano, S. Shiraishi, H. Kurihara, A. Oya, Carbon 41 (2003) 1765–1775.
[79] X. Zhang, S.K. Manohar, Chem. Commun. (2006) 2477–2479.
[80] F. Xu, D. Wu, R. Fu, B. Wei, Mater. Today 20 (2017) 629–656.
[81] M.P. Bichat, E. Raymundo-Piñero, F. Béguin, Carbon 48 (2010) 4351–4361.
[82] E. Raymundo-Piñero, M. Cadek, F. Béguin, Adv. Funct. Mater. 19 (2009) 1032–1039.
[83] V. Presser, M. Heon, Y. Gogotsi, Adv. Funct. Mater. 21 (2011) 810–833.
[84] E.N. Hoffman, G. Yushin, T. El-Raghy, Y. Gogotsi, M.W. Barsoum, Microporous Mesoporous Mater. 112 (2008) 526–532.
[85] M. Oschatz, S. Boukhalfa, W. Nickel, J.P. Hofmann, C. Fischer, G. Yushin, S. Kaskel, Carbon 113 (2017) 283–291.
[86] L. Borchardt, C. Hoffmann, M. Oschatz, L. Mammitzsch, U. Petasch, M. Herrmann, S. Kaskel, Chem. Soc. Rev. (2012).
[87] L. Borchardt, M. Oschatz, S. Kaskel, Mater. Horiz. 1 (2014) 157–168.
[88] M. Oschatz, J.T. Lee, H. Kim, W. Nickel, L. Borchardt, W.I. Cho, C. Ziegler, S. Kaskel, G. Yushin, J. Mater. Chem. A 2 (2014) 17649–17654.
[89] E. Castillo-Martinez, J. Carretero-Gonzalez, J. Sovich, M.D. Lima, J. Mater. Chem. A 2 (2014) 221–228.
[90] J.H. Bitter, J. Mater. Chem. 20 (2010) 7312–7321.
[91] Z. Zhou, C. Lai, L. Zhang, Y. Qian, H. Hou, D.H. Reneker, H. Fong, Polymer 50 (2009) 2999–3006.
[92] J. Bartelmess, S. Giordani, Beilstein J. Nanotechnol. 5 (2014) 1980–1998.
[93] F. Xu, M.-x Wang, Q. Liu, H.-f Sun, S. Simonson, N. Ogbeifun, E.A. Stach, J. Xie, J. Electrochem. Soc. 157 (2010) B1138–B1145.
[94] A. Jain, V. Aravindan, S. Jayaraman, P.S. Kumar, R. Balasubramanian, S. Ramakrishna, S. Madhavi, M.P. Srinivasan, Sci. Rep. 3 (2013) (article 3002).
[95] W. Gu, G. Yushin, Wiley Interdiscip. Rev.: Energy Environ. 3 (2014) 424–473.
[96] M. Inagaki, H. Konno, O. Tanaike, J Power Sources 195 (2010) 7880–7903.
[97] E.T. Mombeshora, V.O. Nyamori, Int. J. Energy Res. 39 (2015) 1955–1980.
[98] K.B. Hatzell, M. Boota, Y. Gogotsi, Chem. Soc. Rev. 44 (2015) 8664–8687.
[99] M. Thommes, K. Kaneko, A.V. Neimark, J.P. Olivier, F. Rodriguez-Reinoso, J. Rouquerol, K.S.W. Sing, Pure Appl. Chem. 87 (2015) 1051–1069.
[100] S. Porada, L. Borchardt, M. Oschatz, M. Bryjak, J.S. Atchison, K.J. Keesman, S. Kaskel, P.M. Biesheuvel, V. Presser, Energy Environ. Sci. 6 (2013) 3700–3712.
[101] S. Kondrat, C.R. Perez, V. Presser, Y. Gogotsi, A. Kornyshev, Energy Environ. Sci. 5 (2012) 6474–6479.
[102] J. Chmiola, G. Yushin, R. Dash, Y. Gogotsi, J Power Sources 158 (2006) 765–772.
[103] I.V. Barsukov, N.A.T. Organization, New Carbon Based Materials for Electrochemical Energy Storage Systems: batteries, Supercapacitors and Fuel Cells, Springer, Dordrecht, 2006.
[104] K. Xia, Q. Gao, J. Jiang, J. Hu, Carbon 46 (2008) 1718–1726.
[105] J. Machnikowski, K. Kierzek, K. Lis, H. Machnikowska, L. Czepirski, Energy Fuels 24 (2010) 3410–3414.
[106] D. Lozano-Castelló, D. Cazorla-Amorós, A. Linares-Solano, Carbon 42 (2004) 1233–1242.
[107] F. Stoeckli, A. Guillot, A.M. Slasli, D. Hugi-Cleary, Carbon 40 (2002) 383–388.
[108] J. Rouquerol, F. Rouquerol, K.S.W. Sing, Adsorption by Powders and Porous Solids: principles, Methodology and Applications, Academic Press, London, 1998.
[109] K. Kaneko, C. Ishii, Colloids and Surfaces 67 (1992) 203–212.
[110] A.M. Puziy, O.I. Poddubnaya, A. Martínez-Alonso, F. Suárez-García, J.M.D. Tascón, Appl. Surf. Sci. 200 (2002) 196–202.
[111] J. Jagiello, J.P. Olivier, Carbon 55 (2013) 70–80.
[112] O. Barbieri, M. Hahn, A. Herzog, R. Kötz, Carbon 43 (2005) 1303–1310.
[113] C.R. Pérez, S.-H. Yeon, J. Ségalini, V. Presser, P.-L. Taberna, P. Simon, Y. Gogotsi, Adv. Funct. Mater. 23 (2013) 1081–1089.
[114] D. Pech, M. Brunet, H. Durou, P. Huang, V. Mochalin, Y. Gogotsi, P.-L. Taberna, P. Simon, Nat. Nanotechnol. 5 (2010) 651–654.
[115] Y. Korenblit, M. Rose, E. Kockrick, L. Borchardt, A. Kvit, S. Kaskel, G. Yushin, ACS Nano 4 (2010) 1337–1344.
[116] H. Gerischer, R. McIntyre, D. Scherson, W. Storck, J. Phys. Chem. 91 (1987) 1930–1935.
[117] D. Weingarth, M. Zeiger, N. Jäckel, M. Aslan, G. Feng, V. Presser, Adv. Energy Mater. (4) (2014) article 1400316..
[118] Z.-S. Wu, K. Parvez, A. Winter, H. Vieker, X. Liu, S. Han, A. Turchanin, X. Feng, K. Müllen, Adv. Mater. 26 (2014) 4552–4558.
[119] J. Tang, J. Liu, C. Li, Y. Li, M.O. Tade, S. Dai, Y. Yamauchi, Angew. Chem. Int. Ed. 54 (2015) 588–593.
[120] S. Zhang, S. Tsuzuki, K. Ueno, K. Dokko, M. Watanabe, Angew. Chem. Int. Ed. 54 (2015) 1302–1306.
[121] L.G. Bulusheva, E.O. Fedorovskaya, A.G. Kurenya, A.V. Okotrub, Phys. Status Solidi (b) 250 (2013) 2586–2591.
[122] J.-K. Ewert, D. Weingarth, C. Denner, M. Friedrich, M. Zeiger, A. Schreiber, N. Jäckel, V. Presser, R. Kempe, J. Mater. Chem. A 3 (2015) 18906–18912.
[123] Y.-H. Lee, K.-H. Chang, C.-C. Hu, J Power Sources 227 (2013) 300–308.
[124] S. Porada, F. Schipper, M. Aslan, M. Antonietti, V. Presser, T.-P. Fellinger, ChemSusChem 8 (2015) 1867–1874.
[125] B. Akinwolemiwa, C. Peng, G.Z. Chen, J. Electrochem. Soc. 162 (2015) A5054–A5059.
[126] T. Brousse, D. Bélanger, J.W. Long, J. Electrochem. Soc. 162 (2015) A5185–A5189.
[127] P. Yang, W. Mai, Nano Energy 8 (2014) 274–290.
[128] A. Laheäär, P. Przygocki, Q. Abbas, F. Béguin, Electrochem. Commun. 60 (2015) 21–25.
[129] T.A. Centeno, O. Sereda, F. Stoeckli, Phys. Chem. Chem. Phys. 13 (2011) 12403–12406.
[130] F. Stoeckli, T.A. Centeno, J. Mater. Chem. A 1 (2013) 6865–6873.
[131] J. Chmiola, G. Yushin, Y. Gogotsi, C. Portet, P. Simon, P.L. Taberna, Science 313 (2006) 1760–1763.
[132] T.A. Centeno, F. Stoeckli, Carbon 48 (2010) 2478–2486.
[133] F. Stoeckli, Russ. Chem. Bull. 50 (2001) 2265–2272.
[134] N. Setoyama, M. Ruike, T. Kasu, T. Suzuki, K. Kaneko, Langmuir 9 (1993) 2612–2617.
[135] N. Setoyama, T. Suzuki, K. Kaneko, Carbon 36 (1998) 1459–1467.
[136] F. Stoeckli, D. Hugi-Cleary, Russ. Chem. Bull. 50 (2001) 2060–2063.
[137] P.A.M. Mourão, P.J.M. Carrott, M.M.L. Ribeiro Carrott, Carbon 44 (2006) 2422–2429.
[138] C. Zhong, Y. Deng, W. Hu, D. Sun, X. Han, J. Qiao, J. Zhang, Electrolytes for Electrochemical Supercapacitors, CRC Press, Boca Raton, 2016.
[139] C.-M. Yang, Y.-J. Kim, M. Endo, H. Kanoh, M. Yudasaka, S. Iijima, K. Kaneko, J. Am. Chem. Soc. 129 (2007) 20–21.
[140] A. Garcia-Gomez, G. Moreno-Fernandez, B. Lobato, T.A. Centeno, Phys. Chem. Chem. Phys. 17 (2015) 15687–15690.
[141] M. Deschamps, E. Gilbert, P. Azais, E. Raymundo-Piñero, M.R. Ammar, P. Simon, D. Massiot, F. Béguin, Nat. Mater. 12 (2013) 351–358.
[142] J.M. Griffin, A.C. Forse, W.-Y. Tsai, P.-L. Taberna, P. Simon, C.P. Grey, Nat. Mater. 14 (2015) 812–819.
[143] H. Wang, T.K.J. Köster, N.M. Trease, J. Ségalini, P.-L. Taberna, P. Simon, Y. Gogotsi, C.P. Grey, J. Am. Chem. Soc. 133 (2011) 19270–19273.
[144] H. Wang, A.C. Forse, J.M. Griffin, N.M. Trease, L. Trognko, P.-L. Taberna, P. Simon, C.P. Grey, J. Am. Chem. Soc. 135 (2013) 18968–18980.
[145] J.M. Griffin, A.C. Forse, H. Wang, N.M. Trease, P.-L. Taberna, P. Simon, C.P. Grey, Faraday Discuss. 176 (2014) 49–68.

[146] W.-Y. Tsai, P.-L. Taberna, P. Simon, J. Am. Chem. Soc. 136 (2014) 8722–8728.
[147] M.D. Levi, S. Sigalov, D. Aurbach, L. Daikhin, J. Phys. Chem. C 117 (2013) 14876–14889.
[148] Q. Dou, L. Liu, B. Yang, J. Lang, X. Yan, Nat. Commun. 8 (2017) (article 2188).
[149] F. Kaasik, T. Tamm, M.M. Hantel, E. Perre, A. Aabloo, E. Lust, M.Z. Bazant, V. Presser, Electrochem. Commun. 34 (2013) 196–199.
[150] M.M. Hantel, V. Presser, R. Kötz, Y. Gogotsi, Electrochem. Commun. 13 (2011) 1221–1224.
[151] M.M. Hantel, D. Weingarth, R. Kötz, Carbon 69 (2014) 275–286.
[152] D. Weingarth, R. Drumm, A. Foelske-Schmitz, R. Kotz, V. Presser, Phys. Chem. Chem. Phys. 16 (2014) 21219–21224.
[153] T. Nishida, Y. Tashiro, M. Yamamoto, J. Fluor. Chem. 120 (2003) 135–141.
[154] W.-Y. Tsai, R. Lin, S. Murali, L. Li Zhang, J.K. McDonough, R.S. Ruoff, P.-L. Taberna, Y. Gogotsi, P. Simon, Nano Energy 2 (2013) 403–411.
[155] R. Lin, P.-L. Taberna, S. Fantini, V. Presser, C.R. Pérez, F. Malbosc, N.L. Rupesinghe, K.B.K. Teo, Y. Gogotsi, P. Simon, J. Phys. Chem. Lett. 2 (2011) 2396–2401.
[156] A. Burke, Electrochim. Acta 53 (2007) 1083–1091.
[157] E.G. Calvo, F. Lufrano, P. Staiti, A. Brigandì, A. Arenillas, J.A. Menéndez, J Power Sources 241 (2013) 776–782.
[158] V. Ruiz, R. Santamaría, M. Granda, C. Blanco, Electrochim. Acta 54 (2009) 4481–4486.
[159] X. Sun, X. Zhang, H. Zhang, D. Zhang, Y. Ma, J. Solid State Electrochem. 16 (2012) 2597–2603.
[160] A. Yu, V. Chabot, J. Zhang, Electrochemical Supercapacitors for Energy Storage and Delivery, CRC Press, Boca Raton, 2013.
[161] L. Demarconnay, E. Raymundo-Piñero, F. Béguin, Electrochem. Commun. 12 (2010) 1275–1278.
[162] K. Fic, G. Lota, M. Meller, E. Frackowiak, Energy Environ. Sci. 5 (2012) 5842–5850.
[163] M. Pourbaix, Atlas of Electrochemical Equilibria in Aqueous Solutions, National Association of Corrosion Engineers, Houston, Texas, 1974.
[164] Q. Gao, L. Demarconnay, E. Raymundo-Pinero, F. Beguin, Energy Environ. Sci. 5 (2012) 9611–9617.
[165] K. Jurewicz, E. Frackowiak, F. Béguin, Appl. Phys. A 78 (2004) 981–987.
[166] F. Endres, A. Abbott, D. MacFarlane, Electrodeposition from Ionic Liquids, Wiley, Weinheim, 2017.
[167] S.-E. Chun, J.F. Whitacre, J Power Sources 242 (2013) 137–140.
[168] F. Béguin, M. Friebe, K. Jurewicz, C. Vix-Guterl, J. Dentzer, E. Frackowiak, Carbon 44 (2006) 2392–2398.
[169] M.J. Bleda-Martínez, J.M. Pérez, A. Linares-Solano, E. Morallón, D. Cazorla-Amorós, Carbon 46 (2008) 1053–1059.
[170] K. Babeł, K. Jurewicz, Carbon 46 (2008) 1948–1956.
[171] R. Ströbel, J. Garche, P.T. Moseley, L. Jörissen, G. Wolf, J Power Sources 159 (2006) 781–801.
[172] K. Jurewicz, E. Frackowiak, F. Béguin, Electrochem. Solid-State Lett. 4 (2001) A27–A29.
[173] M. Hirscher, M. Becher, M. Haluska, A. Quintel, V. Skakalova, Y.M. Choi, U. Dettlaff-Weglikowska, S. Roth, I. Stepanek, P. Bernier, A. Leonhardt, J. Fink, J. Alloy. Compd. 330–332 (2002) 654–658.
[174] B. Fang, H. Zhou, I. Honma, J. Phys. Chem. B 110 (2006) 4875–4880.
[175] Q. Abbas, P. Ratajczak, F. Béguin, Faraday Discuss. 172 (2014) 199–214.
[176] B. Gorska, L. Timperman, M. Anouti, F. Beguin, Phys. Chem. Chem. Phys. 19 (2017) 11173–11186.
[177] P.H. Svensson, L. Kloo, Chem. Rev. 103 (2003) 1649–1684.
[178] V.T. Calabrese, A. Khan, J. Phys. Chem. A 104 (2000) 1287–1292.
[179] G. Lota, E. Frackowiak, Electrochem. Commun. 11 (2009) 87–90.
[180] J. Menzel, K. Fic, M. Meller, E. Frackowiak, J. Appl. Electrochem. 44 (2014) 439–445.
[181] Q. Abbas, F. Béguin, Prog. Nat. Sci.: Mater. Int. 25 (2015) 622–630.
[182] P. Przygocki, Q. Abbas, P. Babuchowska, F. Béguin, Carbon 125 (2017) 391–400.
[183] E. Frackowiak, M. Meller, J. Menzel, D. Gastol, K. Fic, Faraday Discuss. 172 (2014) 179–198.
[184] P. Barpanda, Carbon-Halide Nanocomposites: Structure, Morphology, and Electrochemistry, VDM Publishing, Saarbrücken, 2009.
[185] S. Roldán, M. Granda, R. Menéndez, R. Santamaría, C. Blanco, J. Phys. Chem. C 115 (2011) 17606–17611.
[186] S. Roldán, C. Blanco, M. Granda, R. Menéndez, R. Santamaría, Angew. Chem. Int. Ed. 50 (2011) 1699–1701.
[187] L. Chen, H. Bai, Z. Huang, L. Li, Energy Environ. Sci. 7 (2014) 1750–1759.
[188] P. Ratajczak, K. Jurewicz, P. Skowron, Q. Abbas, F. Béguin, Electrochim. Acta 130 (2014) 344–350.
[189] P. Ratajczak, K. Jurewicz, F. Béguin, J. Appl. Electrochem. 44 (2014) 475–480.
[190] W. Blair John, W. Murphy George, Electrochemical demineralization of water with porous electrodes of large surface area, in: Saline Water Conversion, American Chemical Society, 1960, pp. 206–223.
[191] Y. Liu, C.Y. Nie, X.J. Liu, X.T. Xu, Z. Sun, L.K. Pan, RSC Adv. 5 (2015) 15205–15225.
[192] X. Xu, L. Pan, Y. Liu, T. Lu, Z. Sun, D.H.C. Chua, Sci. Rep. 5 (2015) (article 8458).
[193] R. Zhao, M. Biesheuvel, B. Van der Wal, Energy Environ. Sci. 5 (2012) 9520–9527.
[194] P.M. Biesheuvel, A. van der Wal, J. Membr. Sci. 346 (2010) 256–262.
[195] S. Porada, R. Zhao, A. van der Wal, V. Presser, P.M. Biesheuvel, Prog. Mater. Sci. 58 (2013) 1388–1442.
[196] M.E. Suss, T.F. Baumann, W.L. Bourcier, C.M. Spadaccini, K.A. Rose, J.G. Santiago, M. Stadermann, Energy Environ. Sci. 5 (2012) 9511–9519.
[197] X. Xu, Z. Sun, D.H.C. Chua, L. Pan, Sci. Rep. 5 (2015) (article 11225).
[198] P.M. Biesheuvel, S. Porada, M. Levi, M.Z. Bazant, J. Solid State Electrochem. 18 (2014) 1365–1376.
[199] P.M. Biesheuvel, H.V.M. Hamelers, M.E. Suss, Colloids Interface Sci. Commun. 9 (2015) 1–5.
[200] S. Porada, L. Weinstein, R. Dash, A. van der Wal, M. Bryjak, Y. Gogotsi, P.M. Biesheuvel, ACS Appl. Mater. Interfaces 4 (2012) 1194–1199.
[201] S. Porada, M. Bryjak, A. van der Wal, P.M. Biesheuvel, Electrochim. Acta 75 (2012) 148–156.
[202] E. Avraham, M. Noked, A. Soffer, D. Aurbach, Electrochim. Acta 56 (2011) 6312–6317.
[203] W. Tang, P. Kovalsky, D. He, T.D. Waite, Water Res. 84 (2015) 342–349.
[204] C. Huyskens, J. Helsen, A.B. de Haan, Desalination 328 (2013) 8–16.
[205] T. Kim, J.E. Dykstra, S. Porada, A. van der Wal, J. Yoon, P.M. Biesheuvel, J. Colloid Interface Sci. 446 (2015) 317–326.
[206] C. Prehal, D. Weingarth, E. Perre, R.T. Lechner, H. Amenitsch, O. Paris, V. Presser, Energy Environ. Sci. 8 (2015) 1725–1735.
[207] J. Lee, S. Kim, C. Kim, J. Yoon, Energy Environ. Sci. 7 (2014) 3683–3689.
[208] P. Srimuk, F. Kaasik, B. Kruner, A. Tolosa, S. Fleischmann, N. Jackel, M.C. Tekeli, M. Aslan, M.E. Suss, V. Presser, J. Mater. Chem. A 4 (2016) 18265–18271.
[209] S. Porada, A. Shrivastava, P. Bukowska, P.M. Biesheuvel, K.C. Smith, Electrochim. Acta 255 (2017) 369–378.
[210] X. Gao, S. Porada, A. Omosebi, K.L. Liu, P.M. Biesheuvel, J. Landon, Water Res. 92 (2016) 275–282.
[211] Y. Bouhadana, E. Avraham, M. Noked, M. Ben-Tzion, A. Soffer, D. Aurbach, J. Phys. Chem. C 115 (2011) 16567–16573.
[212] X. Gao, A. Omosebi, J. Landon, K.L. Liu, Energy Environ. Sci. 8 (2015) 897–909.
[213] T. Kim, J. Yoon, RSC Adv. 5 (2015) 1456–1461.
[214] D. Ragone, in: SAE Technical Paper 680453, 1968.
[215] Y. Liu, L. Pan, X. Xu, T. Lu, Z. Sun, RSC Adv. 3 (2013) 16932–16935.
[216] T. Ryu, D.-H. Lee, J.C. Ryu, J. Shin, K.-S. Chung, Y.H. Kim, Hydrometallurgy 151 (2015) 78–83.
[217] W.G. Pell, B.E. Conway, N. Marincic, J. Electroanal. Chem. 491 (2000) 9–21.
[218] R. De Levie, Electrochim. Acta 8 (1963) 751–780.
[219] R. Zhao, P.M. Biesheuvel, H. Miedema, H. Bruning, A. van der Wal, J. Phys. Chem. Lett. 1 (2009) 205–210.
[220] Z.-X. Luo, Y.-Z. Xing, Y.-C. Ling, A. Kleinhammes, Y. Wu, Nat. Commun. 6 (2015) 6358.
[221] M.D. Levi, G. Salitra, N. Levy, D. Aurbach, J. Maier, Nat. Mater. 8 (2009) 872–875.
[222] M.D. Andelman, in: USPTO, 1994.
[223] J. Farmer, in: USP, 1994.
[224] J.C. Farmer, D.V. Fix, G.V. Mack, J.F. Poco, J.K. Nielson, R.W. Pekala, J.H. Richardson, in: Proceedings of the Pacific Rim Environmental Conference, San Francisco, 1995.
[225] D.-K. Kim, T.-H. Kim, C.-H. Cho, C.-S. Park, c. K.-Y., J.-K. Yeo, in: European Patent, 2011.
[226] S.I. Jeon, H.R. Park, J.G. Yeo, S. Yang, C.H. Cho, M.H. Han, D.K. Kim, Energy Environ. Sci. 6 (2013) 1471–1475.
[227] A. Rommerskirchen, Y. Gendel, M. Wessling, Electrochem. Commun. 60 (2015) 34–37.
[228] S. Porada, D. Weingarth, H.V.M. Hamelers, M. Bryjak, V. Presser, P.M. Biesheuvel, J. Mater. Chem. A 2 (2014) 9313–9321.
[229] K.B. Hatzell, E. Iwama, A. Ferris, B. Daffos, K. Urita, T. Tzedakis, F. Chauvet, P.L. Taberna, Y. Gogotsi, P. Simon, Electrochem. Commun. 43 (2014) 18–21.
[230] G.J. Doornbusch, J.E. Dykstra, P.M. Biesheuvel, M.E. Suss, J. Mater. Chem. A 4 (2016) 3642–3647.
[231] Y. Gendel, A.K.E. Rommerskirchen, O. David, M. Wessling, Electrochem. Commun. 46 (2014) 152–156.
[232] T.J. Petek, N.C. Hoyt, R.F. Savinell, J.S. Wainright, J. Electrochem. Soc. 163 (2016) A5001–A5009.
[233] M. Li, H. Hu, H.H. Bau, Phys. Chem. Chem. Phys. 17 (2015) 7181–7195.
[234] T.J. Petek, N.C. Hoyt, R.F. Savinell, J.S. Wainright, J Power Sources 294 (2015) 620–626.
[235] V. Presser, C.R. Dennison, J. Campos, K.W. Knehr, E.C. Kumbur, Y. Gogotsi, Adv. Energy Mater. 2 (2012) 895–902.
[236] L. García-Cruz, P. Ratajczak, J. Iniesta, V. Montiel, F. Béguin, Electrochim. Acta 202 (2016) 66–72.
[237] K.B. Hatzell, M.C. Hatzell, K.M. Cook, M. Boota, G.M. Housel, A. McBride, E.C. Kumbur, Y. Gogotsi, Environ. Sci. Technol. 49 (2015) 3040–3047.
[238] H. Cohen, S.E. Eli, M. Jõgi, M.E. Suss, ChemSusChem 9 (2016) 3045–3048.
[239] K.B. Hatzell, J. Eller, S. Morelly, M. Tang, N.J. Alvarez, Y. Gogotsi, Faraday Discuss. 199 (2017) 511–524.
[240] D.A. Vermaas, S. Bajracharya, B.B. Sales, M. Saakes, B. Hamelers, K. Nijmeijer, Energy Environ. Sci. 6 (2013) 643–651.
[241] S. Loeb, R.S. Norman, Science 189 (1975) 654–655.
[242] J.W. Post, H.V.M. Hamelers, C.J.N. Buisman, Environ. Sci. Technol. 42 (2008) 5785–5790.
[243] R.E. Lacey, Ocean Eng. 7 (1980) 1–47.
[244] D. Brogioli, Phys. Rev. Lett. 103 (2009) (article 058501).
[245] D. Brogioli, R. Ziano, R.A. Rica, D. Salerno, O. Kozynchenko, H.V.M. Hamelers, F. Mantegazza, Energy Environ. Sci. 5 (2012) 9870–9880.
[246] D. Brogioli, R. Ziano, R.A. Rica, D. Salerno, F. Mantegazza, J. Colloid Interface Sci. 407 (2013) 457–466.
[247] D. Brogioli, R. Zhao, P.M. Biesheuvel, Energy Environ. Sci. 4 (2011) 772–777.
[248] R.A. Rica, D. Brogioli, R. Ziano, D. Salerno, F. Mantegazza, J. Phys. Chem. C 116

(2012) 16934–16938.
[249] M. Marino, L. Misuri, M.L. Jiménez, S. Ahualli, O. Kozynchenko, S. Tennison, M. Bryjak, D. Brogioli, J. Colloid Interface Sci. 436 (2014) 146–153.
[250] B. Shapira, E. Avraham, D. Aurbach, ChemSusChem 9 (2016) 3426–3433.
[251] M.C. Hatzell, K.B. Hatzell, B.E. Logan, Environ. Sci. Technol. Lett. 1 (2014) 474–478.
[252] M.C. Hatzell, R.D. Cusick, B.E. Logan, Energy Environ. Sci. 7 (2014) 1159–1165.
[253] S. Ahualli, M.L. Jimenez, M.M. Fernandez, G. Iglesias, D. Brogioli, A.V. Delgado, Phys. Chem. Chem. Phys. 16 (2014) 25241–25246.
[254] S. Lin, A.P. Straub, M. Elimelech, Energy Environ. Sci. 7 (2014) 2706–2714.
[255] A. Punning, V. Vunder, I. Must, U. Johanson, G. Anbarjafari, A. Aabloo, J. Intell. Mater. Syst. Struct. 27 (2016) 1061–1074.
[256] F. Carpi, E. Smela, Biomedical Applications of Electroactive Polymer Actuators, Wiley, Weinheim, 2009.
[257] I. Must, F. Kaasik, I. Põldsalu, U. Johanson, A. Punning, A. Aabloo, Carbon 50 (2012) 535–541.
[258] T. Fukushima, K. Asaka, A. Kosaka, T. Aida, Angew. Chem. 117 (2005) 2462–2465.
[259] B.J. Akle, M.D. Bennett, D.J. Leo, Sens. Actuators A: Phys. 126 (2006) 173–181.
[260] J. Fraysse, A.I. Minett, O. Jaschinski, G.S. Duesberg, S. Roth, Carbon 40 (2002) 1735–1739.
[261] R.H. Baughman, C. Cui, A.A. Zakhidov, Z. Iqbal, J.N. Barisci, G.M. Spinks, G.G. Wallace, A. Mazzoldi, D. De Rossi, A.G. Rinzler, O. Jaschinski, S. Roth, M. Kertesz, Science 284 (1999) 1340–1344.
[262] T. Tsuda, M. Baba, Y. Sato, R. Sakao, K. Matsumoto, R. Hagiwara, S. Kuwabata, Chem. – A Eur. J. 17 (2011) 11122–11126.
[263] Y. Liu, S. Liu, J. Lin, D. Wang, V. Jain, R. Montazami, J.R. Heflin, J. Li, L. Madsen, Q.M. Zhang, Appl. Phys. Lett. 96 (2010) (article 223503).
[264] J. Fraysse, A.I. Minett, G. Gu, S. Roth, A.G. Rinzler, R.H. Baughman, Curr. Appl. Phys. 1 (2001) 407–411.
[265] L. Lu, J. Liu, Y. Hu, Y. Zhang, H. Randriamahazaka, W. Chen, Adv. Mater. 24 (2012) 4317–4321.
[266] P. Viljar, B. Daniel, M. Uno, T. Janno, V. Olga, P. Andres, J. Urmas, K. Maarja, A. Alvo, Smart Mater. Struct. 18 (2009) (article 095028).
[267] J. Torop, V. Palmre, M. Arulepp, T. Sugino, K. Asaka, A. Aabloo, Carbon 49 (2011) 3113–3119.
[268] V. Palmre, E. Lust, A. Janes, M. Koel, A.-L. Peikolainen, J. Torop, U. Johanson, A. Aabloo, J. Mater. Chem. 21 (2011) 2577–2583.
[269] I. Põldsalu, S.-E. Mändmaa, A.-L. Peikolainen, A. Kesküla, A. Aabloo, in: SPIE Smart Structures and Materials + Nondestructive Evaluation and Health Monitoring, SPIE, 2015, p. 10.
[270] R. Siul, M. Benjamin, P. Viljar, J.K. Kwang, Y. Woosoon, Smart Mater. Struct. 24 (2015) 015007.
[271] K. Takahashi, M. Fukano, S. Yoshida, M. Ogawa, F. Kusu, Anal. Sci. 28 (2012) 853–859.
[272] R.S. Deinhammer, E.Y. Ting, M.D. Porter, Anal. Chem. 67 (1995) 237–246.
[273] B.J. Yakes, D.W. Keller, M.D. Porter, J. Chromatogr. A 1217 (2010) 4395–4401.
[274] E.Y. Ting, M.D. Porter, J. Electroanal. Chem. 443 (1998) 180–185.